

AD A047407

12

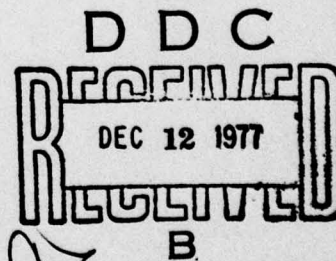
AD-E000019

NRL Memorandum Report 3580

**DARPA-NRL Laser Program  
Semiannual Technical Report to  
Defense Advanced Research Projects Agency  
1 October 1976—30 March 1977**

*Laser Physics Branch  
Optical Sciences Division*

September 1977



AD No. \_\_\_\_\_  
DDC FILE COPY

**NAVAL RESEARCH LABORATORY  
Washington, D.C.**

Approved for public release; distribution unlimited.

14 NRL-MR-3580

SECURITY CLASSIFICATION OF THIS PAGE (When Data Entered)

REPORT DOCUMENTATION PAGE		READ INSTRUCTIONS BEFORE COMPLETING FORM
1. REPORT NUMBER NRL Memorandum Report 3580	2. GOVT ACCESSION NO.	3. RECIPIENT'S CATALOG NUMBER 9 Interim rept.
4. TITLE (and Subtitle) DARPA-NRL LASER PROGRAM - SEMIANNUAL TECHNICAL REPORT TO DEFENSE ADVANCED RESEARCH PROJECTS AGENCY - 1 October 1976 - 30 March 1977		5. TYPE OF REPORT & PERIOD COVERED Interim report on a continuing NRL problem.
7. AUTHOR(s) Laser Physics Branch Optical Sciences Division		6. PERFORMING ORG. REPORT NUMBER
9. PERFORMING ORGANIZATION NAME AND ADDRESS Naval Research Laboratory Washington, D.C. 20375		8. CONTRACT OR GRANT NUMBER(s) 15 DARPA Order - 2062
11. CONTROLLING OFFICE NAME AND ADDRESS Defense Advanced Research Projects Agency Arlington, Virginia 22209		10. PROGRAM ELEMENT PROJECT, TASK AREA & WORK UNIT NUMBERS NRL Problem K03-53 Project 7E20
14. MONITORING AGENCY NAME & ADDRESS (if different from Controlling Office)		12. REPORT DATE Sep 1977
		13. NUMBER OF PAGES 82 12 84p.
		15. SECURITY CLASS. (of this report) UNCLASSIFIED
		15a. DECLASSIFICATION DOWNGRADING SCHEDULE
16. DISTRIBUTION STATEMENT (of this Report) Approved for public release; distribution unlimited. 18 SBIE		
17. DISTRIBUTION STATEMENT (of the abstract entered in Block 20, if different from Report) 19 AD-E000019		
18. SUPPLEMENTARY NOTES		
19. KEY WORDS (Continue on reverse side if necessary and identify by block number) Lasers Electrical lasers Laser diagnostics Electronic state lasers Chemical kinetics Electronic state lifetimes Energy transfer Chemiluminescence		
20. ABSTRACT (Continue on reverse side if necessary and identify by block number) The DARPA-NRL Laser Program is concerned with the development of laser technology of electronic state lasers and associated physics. In particular the development of the XeF laser has been emphasized. Experimental and theoretical efforts were made to understand and improve laser performance. The radiative lifetime of XeF was measured by photolytic dissociation of XeF <sub>2</sub> . A short pulse electron beam device was set up to remeasure the XeF lifetime more accurately and work was started to synthesize KrF <sub>2</sub> in order to measure the lifetime of KrF. Values for the radiative (Continues)		

DD FORM 1473 1 JAN 73

EDITION OF 1 NOV 65 IS OBSOLETE  
S/N 0102-014-6601

SECURITY CLASSIFICATION OF THIS PAGE (When Data Entered)

251 950 22

## 20. Abstract (Continued)

lifetime are used in a code to predict laser performance of both XeF and KrF. Experimentally the performance of the XeF laser has been improved. Long laser pulses were observed for the first time and laser efficiency was increased by substitution of Ne for Ar, the diluent. Absorption measurements combined with code calculations showed that the improvement was due to decreased dimer ion optical absorption.

In other work, the output of the XeF laser at 351 nm was converted to 585 nm which has a more favorable atmospheric propagation. The photon conversion of 90% is higher than ever obtained before by a resonance Raman scheme which is scalable to high power operation. Finally, the 50 ns NRL electron beam gun was used to investigate the new HgCl laser. Improvements were also made on the heated cell for rare gas-alkali new laser experiments.

RECEIVED for	
NTIS	White Section <input checked="" type="checkbox"/>
DDC	B.N. Section <input type="checkbox"/>
UNANNOUNCED	<input type="checkbox"/>
JUSTIFICATION	
BY	
DISTRIBUTION/AVAILABILITY CODES	
Dist.	ARL and/or SPECIAL
A	

## CONTENTS

FOREWORD	iv
ELECTRONIC STATE LASERS	
1. Radiative Lifetime Measurements of XeF and KrF	1
2. XeF and KrF Laser Computer Models	15
3. XeF Laser Performance from the Maxwell Cold Cathode Electron Beam Device	22
4. Raman Shifting of Rare Gas Halide Laser Emission	43
5. Progress in New Lasers with the NRL 50 ns Electron Beam Apparatus	56

# FOREWORD

The Laser Physics Branch of the Optical Sciences Division, Naval Research Laboratory, Washington, D. C., prepared this semiannual report on work sponsored by the Defense Advanced Research Projects Agency, DARPA Order 2062. The projects described are also funded by NRL-ONR research funds. Co-authors of the report were R. Burnham, L. Champagne, N. Djeu, J. G. Eden, N. W. Harris, S. K. Searles, W. S. Watt, and B. Wexler.

..

SEMIANNUAL TECHNICAL REPORT

REPORTING PERIOD

1 October 1976 - 30 March 1977

1. DARPA Order	2062, Amendments 12 & 15
2. Program Code Number	7E20
3. Name of Contractor	Naval Research Laboratory
4. Effective Date of Contract	1 July 1972
5. Contract Expiration Date	30 September 1977
6. Amount of Contract	\$339,000
7. Contract Number	62301E
8. Principal Investigator	W. S. Watt
9. Telephone Number	(202) 767-3217
10. Project Scientist	S. K. Searles
11. Telephone Number	(202) 767-2255
12. Title of Work	DARPA/NRL Laser Technology Program

SPONSORED BY

DEFENSE ADVANCED RESEARCH PROJECTS AGENCY

DARPA Order No. 2062

DARPA-NRL LASER PROGRAM SEMIANNUAL TECHNICAL REPORT  
TO DEFENSE ADVANCED RESEARCH PROJECTS AGENCY  
1 October 1976 - 30 March 1977

ELECTRONIC STATE LASERS

1. Radiative Lifetime Measurements of XeF and KrF

The radiative lifetime of a laser species is a key parameter needed to predict laser performance. We have improved lifetime measurements in order to make reliable laser predictions. Previously we determined the lifetime to be  $16.5 \pm 5$  ns with the use of a 50 ns FWHM long electron beam excitation pulse. It is desirable, however, to use a source with a shorter pulse duration. The following describes the use of a laser excitation source with a 15 ns pulse duration. After the laser excitation source results, plans to use a 3 ns electron beam device are discussed. The 3 ns device will permit a marginal improvement in the XeF lifetime measurement and, more important, will allow measurement of the KrF lifetime which is only 6.7 ns according to theoretical calculations. The lifetime of KrF has not yet been measured experimentally.

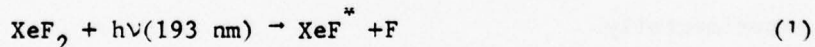
The radiative lifetime of the excited state of the 351 nm laser transition in XeF has been measured by employing a new technique in which a parent molecule ( $\text{XeF}_2$ ) was dissociatively photoexcited using a pulsed laser photolysis source. The laser was a discharge-pumped argon fluoride laser which emitted pulses with intensities of approximately one megawatt/cm<sup>2</sup> at a wavelength of 193 nm. At this

---

Note: Manuscript submitted August 2, 1977.

wavelength the energy of the laser photons (6.4 eV) is sufficient to dissociate the xenon difluoride molecule ( $D(\text{XeF-F}) = 2.6 \text{ eV}$ ) leaving the product XeF in the excited state of the laser transition. Radiation from this state at 351 nm was followed by a fast photodetector in order to determine the lifetime of the excited xenon fluoride molecule. The laser photolysis technique permitted an unequivocal determination of the XeF lifetime since the fluorescence cell in which the experiment was conducted contained only the parent  $\text{XeF}_2$  molecule at a low pressure together with a negligible concentration of photofragments produced by the photolysis. The experiment was therefore free of complications arising from the presence of charged particles and buffer gasses usually present when electron impact excitation is used to produce the excited species.

Details of the lifetime experiment are contained in the following article [Radiative Lifetime of the C State of XeF]. The lifetime of the excited XeF ( $\text{XeF}^*$ ) was obtained from the fluorescence at 351 nm under the assumption of a single step process:



followed by radiative or collisional decay:



By varying the pressure of  $\text{XeF}_2$  in the experimental cell the contribution to the decay of the 351 nm fluorescence due to radiative and collisional processes could be separated. A typical fluorescence

trace showing the temporal shapes of the 193 nm pump pulse, the resulting fluorescence at 351 nm, and the theoretical fitted pulse shapes is given in Fig. A.

Results of the present experiment give a value of 18.8 nsec for the lifetime of  $\text{XeF}^*$ , and a rate of  $3.5 \times 10^{-10} \text{ cm}^3/\text{sec}$  for quenching of  $\text{XeF}^*$  by  $\text{XeF}_2$ . The value of the lifetime has found immediate application to the calibration of quenching data for  $\text{XeF}$  obtained by Setser et al. using a Stern-Volmer technique. Further, the lifetime data allows the cross-section for stimulated emission in  $\text{XeF}$  to be calculated accurately from measured linewidths for the first time. Knowledge of the stimulated emission cross-section is, of course, essential to laser efficiency modelling.

Presently the photolysis experiments described above are being continued in order to measure two and three body rates for quenching of  $\text{XeF}^*$  and ground state  $\text{XeF}$  by molecules encountered in typical laser gas mixtures. These measurements will provide an independent set of quenching data obtained using the most direct and accurate experimental technique presently available.

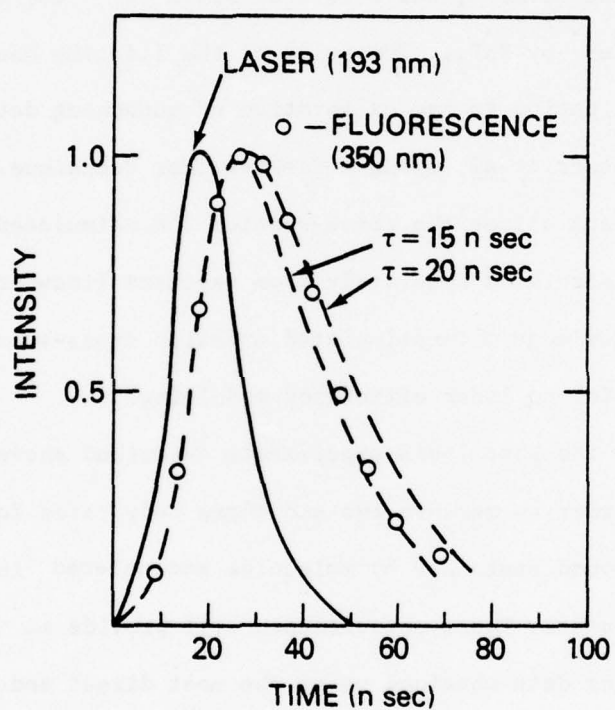


Figure A. Comparison of experimental fluorescence curve and fitted curve for XeF from photolyzed XeF<sub>2</sub>.

# RADIATIVE LIFETIME OF THE C STATE OF XeF

R. Burnham\* and N. W. Harris

..

\*Science Applications Incorporated, Arlington, VA 22202

The radiative lifetime of the upper state of the 350 nm transition in  $\text{XeF}^1$  has been measured in  $\text{XeF}$  excited through dissociative photoexcitation of  $\text{XeF}_2$  vapor at 193 nm. Dissociating radiation was obtained from a discharge pumped ArF laser, which supplied optical pulses of 16 nsec duration with peak intensities of about  $1 \text{ MW/cm}^2$ .<sup>2</sup> Excitation of the C state in  $\text{XeF}$  appears to result from a single step dissociation of  $\text{XeF}_2$  upon absorption at 193 nm. Absorption spectra of  $\text{XeF}_2$  in this region show a strong absorption band centered at 158 nm.<sup>3</sup> Details of the photodissociation mechanism in  $\text{XeF}_2$  are not known. The energy of the 193 nm photon is, however, sufficient to dissociate  $\text{XeF}_2$  [ $D(\text{XeF-F}) \approx 2.6 \text{ eV}$ ]<sup>4</sup> leaving the product  $\text{XeF}$  in the C State at 3.5 eV.

Photolysis of  $\text{XeF}_2$  was carried out in a cylindrical quartz fluorescence cell with a length of 10 cm and a diameter of 2.5 cm. Fluorescence was observed at  $90^\circ$  to the incident radiation at a position directly behind the entrance window. The pressure of  $\text{XeF}_2$  in the cell was controlled by the saturated vapor pressure of  $\text{XeF}_2$  contained in a side-arm which was maintained at a uniform temperature. The  $\text{XeF}_2$  pressure was calculated from the data of Schreiner, McDonald, and Chernick.<sup>5</sup> During an experimental run the temperature of the sidearm was allowed to increase from approximately 265 to 290 K over the period of about 0.5 h. The corresponding increase in vapor pressure was from 0.26 to 2.6 Torr. Before each experimental run the cell was pumped to a background pressure of  $< 1 \mu$  through a trapped line and sealed.

Survey spectra of the fluorescence from  $\text{XeF}_2$  pumped at 193 nm were taken using a 1/4-m spectrometer and photomultiplier. Strong fluorescence was observed at 350 nm and weak fluorescence was observed on a broad band centered at  $\sim 450$  nm. No other emission was detected between 200 and 800 nm. Specifically the  $\text{XeF}$  (D-X) emission at 260 nm was not detected. High resolution spectra of the 350 nm fluorescence revealed a broad ( $\Delta\lambda \approx 15$  nm) but structured band similar to the  $\text{XeF}$  (C-X) band observed in low pressure flowing afterglows<sup>6</sup> and low pressure discharges in Xe and  $\text{F}_2$ . The 350 nm fluorescence was therefore attributed to the (C-X) laser transition in  $\text{XeF}$ .

The lifetime of the photolytically formed  $\text{XeF}$  (C) state was obtained directly from the decay of the 350 nm fluorescence. For the purpose of the lifetime measurement a fast vacuum photodiode and 350 nm filter were substituted for the photomultiplier and monochromator used for the fluorescence survey spectra. The filter was centered at a wavelength of 350 nm and had a fairly flat-topped band-pass with a half-width of 817 nm. Decay curves were taken directly from oscilloscope traces. The response time for the detector-oscilloscope was less than 1 nsec. The lifetime of the  $\text{XeF}$  (C) state ( $\text{XeF}^*$ ) was obtained from the fluorescence traces under the assumption of a single step excitation process followed by radiative or collisional decay. The rate equation for  $\text{XeF}^*$  is then

$$\frac{d[\text{XeF}^*]}{dt} = P(t) - [\text{XeF}^*] \left( \frac{1}{\tau} + k_q [\text{XeF}_2] \right), \quad (1)$$

where  $k_q$  is the rate constant for quenching of  $\text{XeF}_2$  and  $\tau$  is the

radiative lifetime. The appropriate solution of Eq. (1) is

$$[\text{XeF}^*] = ce^{-At} \int_0^t P(x)e^{Ax} dx, \quad (2)$$

where A is the total transition rate given by

$$A = (1/\tau + k_q [\text{XeF}_2]). \quad (3)$$

The source term P(t) was obtained from the temporal shape of the 193 nm laser pulse measured simultaneously with the 350 nm fluorescence. The absorption is not expected at the pump intensities employed in the present experiment. Thus the pumping rate should be directly proportional to the pump intensity at 193 nm.

Fluorescence data taken at pressures above 0.5 Torr were sufficiently free of spurious noise that the decaying part of the fluorescence could be fitted to a single exponential decay over approximately 2 e-foldings following the termination of the pump pulse. In all cases excellent fits with simple exponential decays were obtained.

Data taken at pressures below 0.5 Torr were sufficiently noisy to require fitting of the fluorescence over the entire pulse. For this purpose Eq. (2) was solved numerically for several values of the parameter A in the range of the expected decay rate. Fluorescence curves were then fitted graphically to the numerical solutions. The error in the values of the transition rates obtained in this way is estimated to be about 20% per experimental point.

The fluorescence decay rates are plotted in Fig. 1 as a function

of the pressure of  $\text{XeF}_2$  in the fluorescence cell. The zero-pressure intercept of the fitted line gives a lifetime for the C state of  $\text{XeF}$  of 18.8 nsec. The rate constant for the quenching of  $\text{XeF}$  (C) by  $\text{XeF}_2$  is found from the slope of the line in Fig. 1 to be  $3.5 \times 10^{-10} \text{ cm}^3 \text{ sec}^{-1}$ . The rms error for both quantities is about 7%. The absolute value of the quenching rate constant depends on the accuracy of vapor pressure data for  $\text{XeF}_2$ . Uncertainty in the quenching rate will, however, introduce a much smaller uncertainty into the value of the lifetime. The lifetime obtained in the present experiment agrees well with the value of  $16 \pm 5$  nsec obtained by Eden and Searles<sup>7</sup> from fluorescence decay measurements using  $\text{XeF}_2$  dissociatively excited in an electron beam.

In the present experiments no attempt has been made to spectrally resolve fluorescence originating from different excited state vibrational levels. Implicit in our results, then, is the assumption that the lifetimes of the vibrational states contributing to the fluorescence are equal. The simple exponential decay of the fluorescence and the linear dependence on the density of  $\text{XeF}_2$  of the fluorescence decay rate shown in Fig. 1 are both consistent with the above assumption.

### References

1. The designation of the electronic states of XeF follows that of T. H. Dunning, Jr., and P. J. Hay, Appl. Phys. Lett. 28, 649 (1976).
2. R. Burnham and N. Djeu, Appl. Phys. Lett. 29, 707 (1976).
3. J. Jortner, E. G. Wilson, and S. A. Rice in Noble Gas compounds, edited by H. H. Hayman (University of Chicago Press, Chicago, 1963), p. 358.
4. J. Berkowitz, W. A. Chupka, P. M. Cuyon, J. H. Holloway, and R. Spohr, J. Phys. Chem. 75, 1461 (1971).
5. F. Schreiner, G. N. McDonald, and C. L. Chernick, J. Phys. Chem. 72, 1162 (1968).
6. J. E. Velazco, J. H. Kolts, and D. W. Setser, J. Chem. Phys. 65, 3468 (1976).
7. J. G. Eden and S. K. Searles (unpublished).

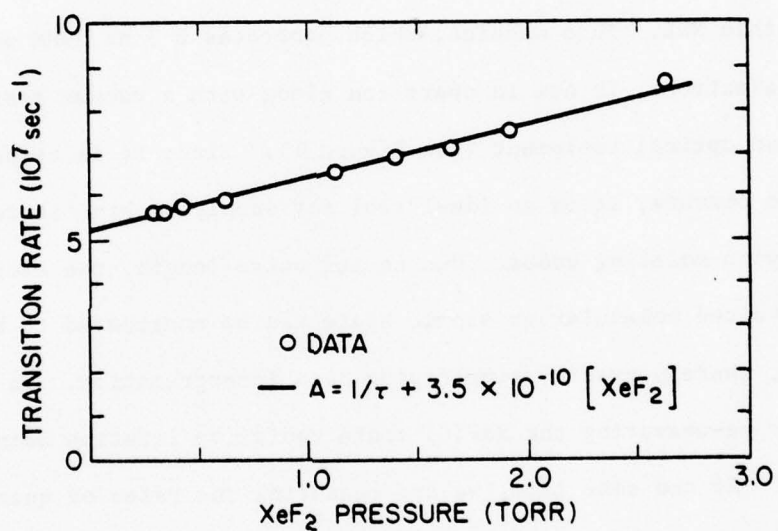


Figure 1. Rate of decay of the XeF(C) state vs the pressure of XeF<sub>2</sub> in the fluorescence cell. The zero-pressure intercept of the fitted line gives a values of 18.8 nsec for  $\tau$ , the XeF(C) state lifetime.

Last Fall we successfully measured the radiative lifetime of  $\text{XeF}(\text{C})$  to be  $16.5 \pm 5$  ns by dissociating  $\text{XeF}_2$  with an e-beam. However, the pulse length of the machine used is 50 ns FWHM. It is desirable, when measuring rates of this nature, to use an electron source which has a pulse length  $\ll \tau_{\text{rad}}$  17 ns.

A Febetron 706 e-beam gun was recently acquired from another group within NRL. This machine, which generates a 3 ns FWHM pulse of 600 Kev electrons, is now in operation along with a vacuum system and associated optical equipment (see Figure B). Since it is compact and simple to operate, it is an ideal tool for supplying kinetic rates necessary to modeling codes. Due to its pulse length, the excitation of the desired molecular or atomic state can be considered to be a  $\delta$  - function, thereby greatly simplifying data interpretation. We are currently re-measuring the  $\text{XeF}(\text{C})$  state radiative lifetime using the Febetron. At the same time, we are measuring the rates of quenching of  $\text{XeF}^*$  by rare gases and halogen donors such as  $\text{XeF}$ ,  $\text{NF}_3$ , etc. These cross-sections are of great value to our computer modeling studies and the efforts to scale up the  $\text{XeF}$  laser.

We are also preparing  $\text{KrF}_2$  in an effort to extend these measurements to the  $\text{KrF}^*(\text{C})$  molecule. Present plans call for completing this study within the next 3 months.

Finally, due to the attractive features of the  $\text{HgX}^*$  laser family, investigations of the radiative lifetimes and rates of quenching of  $\text{HgX}(\text{B}^2\Sigma)$  molecules by  $\text{Hg}$ ,  $\text{X}_2$  and the rare gases would be valuable. By

dissociating the appropriate mercury salt,  $\text{HgX}_2$ , by an e-beam (or KrF laser) in the presence of a quenching gas, such measurements would be straightforward.

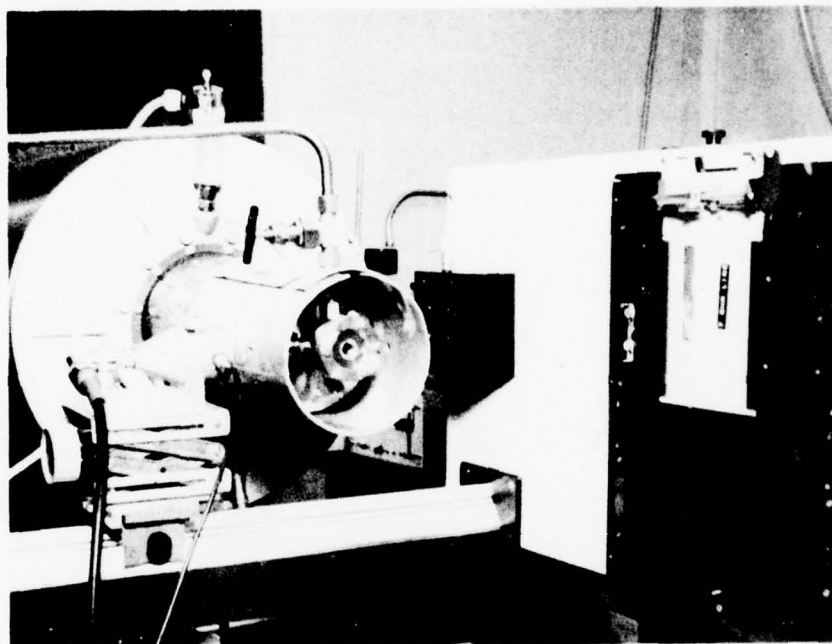


Figure B. Febetron 706 gun with stainless steel sample cell attached. Gun generates a 3 ns pulse at 600 KV and 10 KA. Viewing parts allow temporal and spectral analysis of the sample emission.

## 2. XeF and KrF Laser Computer Models

A numerical modeling effort was initiated during this reporting period to provide guidance for several of the present experiments and to aid in interpreting their results. The general approach followed by this effort has been to keep the computer codes simple, flexible, modular, and inexpensive to allow the modeling of a variety of laser systems and laser related experiments. The codes have thus far been designed around the modeling of rare gas halide lasers pumped by an electric discharge, an electron beam, UV photons, or a combination of these; they are also suitable for modeling experiments designed to measure reaction rates important in rare gas halide lasers and have been applied to experiments involving fluorescence measurements of e-beam excited gas mixtures and to transient photoabsorption measurements of laser gases. The work discussed here is aimed at developing the numerical capability of modeling (a) excitation and ionization of laser gas mixtures by electric discharges, (b) the time varying chemical reaction kinetics during and following such excitation, (c) the extraction of laser energy from such excited mixtures. Additionally, since the results of the model are only as good as the input an up to date file of measured and calculated reaction rates, cross sections, and lifetimes for the relevant species must be maintained.

### Kinetics Package

Much of the time and effort spent during this reporting period was dedicated to the development of a useful code for solving a set

of coupled differential equations describing the behavior of a particular laser gas mixture under specified excitation conditions. The emphasis was placed here because the kinetics package alone (when merged with an existing e-beam deposition code) could be used to model e-beam pumped rare-gas halide lasers currently being studied in the laboratory.

The core of the kinetics package is a somewhat modified version of a general purpose Runge-Kutta-Treanor<sup>1</sup> algorithm for solving a set of coupled differential equations with greatly different time constants such as are commonly encountered in chemical kinetics modeling. To this core was added a bookkeeping procedure which handles reactions written in symbolic format on data cards and translates them into the corresponding set of coupled first order differential equations. Also, coding to print out relevant information such as population densities, their time derivatives, reaction rates, and rate constants has been developed. The bookkeeping feature eliminates errors frequently introduced when translating a large number of reactions into rate equations. It also allows easy removal, addition, and modification of selected reactions and rate constants thus facilitating variation of these quantities from one computer run to the next to determine their effect on predicted laser output and efficiency. The printing out of selected intermediate results is useful in gaining insight into the important kinetic processes and in determining which reactions (e.g., formation, quenching, precursor interception, bottlenecking, etc.) are most

important to produce lasing for a given set of initial conditions. Additional output is provided to check the numerical accuracy of the integration.

The chemical kinetics package has been amended to include the computation of the time-dependent density of lasing and fluorescence photons. Thus the total laser energy, laser output power, cavity flux, laser energy absorption, and fluorescence intensity are available from the code printout. From these data, laser efficiency can easily be calculated.

#### Boltzmann Code

A computer routine for modeling the behavior of a weakly ionized gas mixture in a constant (or slowly varying) electric field was developed by T. H. Johnson of Air Force Weapons Laboratory. This code solves the Boltzmann transport equation for the electron distribution function in a specified gas mixture accounting for momentum transfer, inelastic, superelastic, and attachment collisions between the electrons and the gas constituents. Reaction rates obtained by convolving the electron energy distribution function with tabulated cross sections are computed at each time step and fed to the kinetics package. The Boltzmann code was recently converted to run on the Texas Instruments ASC computer at NRL. The converted version has been successfully tested on a helium-krypton gas mixture and (after some revisions to decrease its run time on the ASC) will soon be linked to the kinetics package described above to provide the capability of

modeling e-beam sustained laser systems.

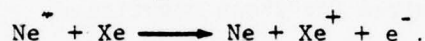
#### Modeling of Transient Absorption

The kinetics package has been used to model e-beam pumped pure Ar and Ne as well as Ar/Xe and Ne/Xe mixtures. The results<sup>2</sup> of this modeling have aided in explaining recent NRL experiments<sup>3</sup> which showed that substitution of neon for argon as the diluent gas substantially improved XeF laser performance through a reduction in absorption at the 351.1 nm lasing wavelength. The time dependent population densities computed by the model were compared with transient photoabsorption measurements on electron beam excited gas mixtures to determine the mechanism for strong absorption in the argon diluent case and weak absorption in the neon diluent case.

The model has shown that when small amounts of Xe are added to pure Ne, a substantial reduction in the transient concentrations of the suspected absorbers  $\text{Ne}_2^+$  and  $\text{Ne}_3^+$  occurs. For example, Fig. C shows computed population densities of  $\text{Ne}_2^*$  and  $\text{Ne}^+$  for 5 atm of pure Ne (solid curves) and for Ne with 0.2% Xe. (dashed curve). With Xe added, the computed population density of  $\text{Ne}_2^+$  drops by more than a factor of 2 during the e-beam pulse while the population density of  $\text{Ne}_2^*$  stays about the same with or without the Xe additive (The corresponding dashed curve for  $\text{Ne}_2^*$  with Xe added is not shown since it almost exactly overlaps the solid curve). The measurements show a reduction in absorption comparable to the computed reduction in concentration of the  $\text{Ne}_2^+$ . Similar computations for pure Ar and Ar/Xe

'mixtures show only a slight reduction in the  $\text{Ar}_2^+$  concentrations when Xe is added and this compares well with measurements which show only a small reduction in transient absorption for the Ar/Xe case vs. the pure Ar case.

The model has shown that a key reaction resulting indirectly in reduction of the  $\text{Ne}_2^+$  and  $\text{Ne}_3^+$  population density is Penning ionization:



Because Penning ionization of Xe by excited Ar is not energetically allowed, no substantial reduction of the  $\text{Ar}_2^+$  concentration is predicted for the Ar-Xe mixtures.

#### Planned Improvements and Applications

Near-term goals for modeling of transient absorption in XeF lasers are the extension of the modeling to Ar/Xe/NF<sub>3</sub> and Ne/Xe/NF<sub>3</sub> mixtures for pumping by e-beam only and for e-beam sustained discharges. The application of the kinetics package with laser energy extraction to actual XeF lasing mixtures should not only clarify the optical absorption mechanisms (measurements show that laser light absorption is even further reduced for Ne/Xe/NF<sub>3</sub> mixtures compared with pure Ne and Ne/Xe mixtures) but also should elucidate which mechanisms are most important in producing optimum output power and efficiency in XeF lasers. To model sustained discharges, the kinetics package must be linked to Johnson's Boltzmann transport equation solver. This linkage plus associated optimization and testing are planned for the next few months.

It is also planned to modify the output of the kinetics package to provide information which will aid in determining which reactions and processes are most effective in enhancing or limiting laser performance for a given set of initial conditions. This information is important to indicate which reactions, cross sections and lifetimes are most in need of measurement or calculation and should also provide as estimate of the accuracy required for these quantities.

#### References

- <sup>1</sup> Charles E. Treanor, CAL Report No. AG-1729-A-4 (Cornell Aeronautical Laboratory, Jan. 1964)
- <sup>2</sup> L. J. Palumbo and L. F. Champagne, "Optical Absorption in a XeF Laser," presented as a post deadline paper at the Fifth Conference on Chemical and Molecular Lasers, St. Louis, Mo. (April 18-20, 1977).
- <sup>3</sup> L. F. Champagne and N. W. Harris, to be published in Applied Physics Letters, 1977.

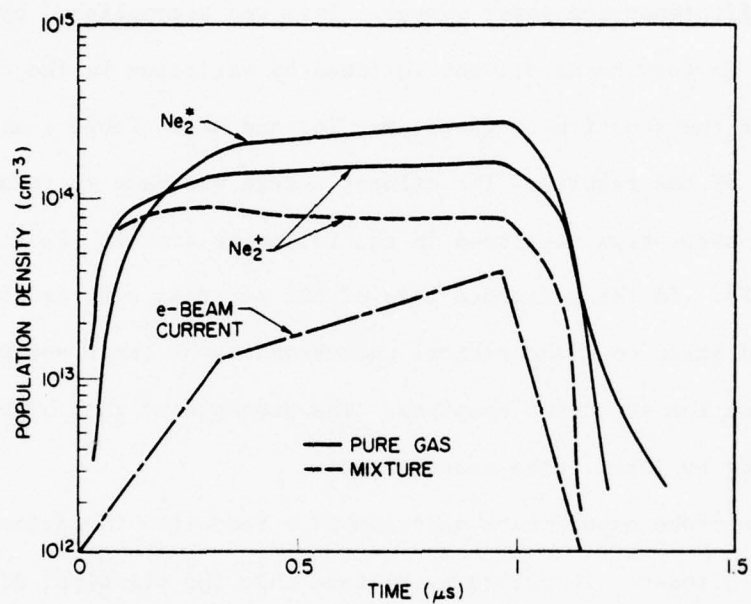


Figure C. Calculated population densities of  $\text{Ne}_2^+$  and  $\text{Ne}_2^*$  for e-beam excited pure Ne (solid curves and Ne = 0.2% Xe (dashed curve) vs. time.

### 3. XeF Laser Performance from the Maxwell Cold Cathode Electron Beam Device

Previously we advanced XeF laser technology through the development of long laser pulse operation. Now we report improvement of the laser efficiency and power output. This was accomplished by substitution of Ne for the Ar diluent followed by variation in the concentrations of the substituent gases, Ne, Xe, and  $\text{NF}_3$ . Table I shows a summary of the results. The diluent change was made to reduce transient optical absorption mentioned in the following article [1- $\mu\text{s}$  Laser Pulses from XeF]. In the article a loss of 50% per pass with Ar diluent was reported based on a theoretical understanding of laser power output as a function of output coupling. The presence of this high loss was confirmed by laser probe measurements.

The probe experiments also showed a reduction in optical loss with Ne as a diluent. Therefore we believe that the principal effect of the diluent change is a reduction of transient optical absorption. The probe results are fully described in the second article [The Influence of Diluent Gas on the XeF Laser].

Table I

Characteristics of the XeF Laser  
with 100 cm active path length

A. Laser Performance			
Optimum Gas Composition		<u>Ar Diluent</u>	<u>Ne Diluent</u>
Diluent		99.52	99.76
Xe		0.36	0.18
NF <sub>3</sub>		0.12	0.06
Pressure with Equal Input Energy		2.5 atm	5.0 atm
Specific Energy from 387 cm <sup>3</sup>		0.8 J/l	2.8 J/l
Efficiency based on deposited energy		0.5%	1.8%
Maximum Optical Pulse Length		1.5 $\mu$ sec	3.5 $\mu$ sec
Threshold Pumping Current Density		8.2 A/cm <sup>2</sup>	1.2A/cm <sup>2</sup>
B. Probe Results in %/cm			
Gain at 351 nm		1.50	1.35
Loss at 337.8 and at 363.8 nm		<u>0.35</u>	<u>0.07</u>
Gain minus loss		1.15	1.28

1- $\mu$ s LASER PULSES FROM XeF  $\pm$

L. F. Champagne, J. G. Eden,  
N. W. Harris, N. Djeu, and S. K. Searles

Appl. Phys. Lett. 30, 160 (1977).

Abstract

Long-pulse operation of the XeF laser has been achieved utilizing electron beam excitation of Ar/Xe/NF<sub>3</sub> gas mixtures. For a total mixture pressure of 2.5 atm,  $\sim 0.30$  J of 350-nm radiation was obtained in a 1- $\mu$ s FWHM pulse.

$\pm$  Work supported in part by DARPA

The performance of rare-gas halide lasers has been considerably improved since their discovery less than two years ago.<sup>1</sup> Advances in laser peak power and efficiency have been demonstrated. However, laser pulse duration has been restricted to less than 220 nsec (KrF).<sup>2</sup> For some applications long-duration pulses are required. We report observation of long essentially cw laser pulses from XeF with electron beam (e-beam) pumping. These pulses, up to 1.5  $\mu$ s, are a factor of 15 longer than previously reported for XeF.<sup>3</sup>

A diagram of the laser cell is shown in Fig. 1. A Maxwell cold-cathode electron gun<sup>4</sup> was used to generate 300-keV electrons. The current density at the 25- $\mu$ -thick Ti foil was 14 A/cm<sup>2</sup> for a 1.2- $\mu$ s FWHM pulse, 8 A/cm<sup>2</sup> for 1.5  $\mu$ s, and 5.2 A/cm<sup>2</sup> for 2  $\mu$ s. The reduction in current density results from the greater anode-cathode spacing required for the longer pulse lengths. The electron beam entered the laser cell with a rectangular cross section of 2.6 cm x 100 cm.

Laser energy was extracted from a cylindrical volume 100 cm long and 2.22 cm in diameter. Optical-quality CaF<sub>2</sub> or fused silica windows were installed at Brewster's angle. Dielectric-coated mirrors of 3 m radius of curvature separated by 2 m formed the laser cavity. One mirror was >99% reflecting. The reflectance of the output mirror or quartz flat can be read from the abscissa of Fig. 3. Laser energy coupled out of the laser resonator was measured by a Gen-Tec ED-500 pyroelectric detector. Laser power was measured by directing 10% of the power output to an S-5 F4018 photodiode detector. The Ar and Xe

were research grade, while the  $\text{NF}_3$  was commercial quality, 98% pure. In a few experiments  $\text{F}_2$  (98% pure) was substituted for  $\text{NF}_3$ . As expected  $\text{NF}_3$  gave better laser performance than  $\text{F}_2$ .

The partial pressures of Ar, Xe, and  $\text{NF}_3$  were varied to get optimum laser efficiency with 1.2 - 1.4- $\mu\text{s}$  e-beam excitation pulses. A mixture of Ar (99.5%), Xe (0.38%), and  $\text{NF}_3$  (0.12%) gave the highest energy, 300 mJ at 2.5 atm total pressure. The optimum gas composition did not change with pressure. At the lowest pressure (1 atm) the energy dropped to 200 mJ and at the highest pressure (5 atm) the energy was 36 mJ. Over most of this range the pulse was 1  $\mu\text{s}$  long.

Figure 2 shows typical oscilloscope traces of the laser and e-beam current waveforms. The beam current has been normalized, unity corresponding to a current density of 11  $\text{A}/\text{cm}^2$ . It can be seen that laser emission occurred as long as the current density exceeded 8.5  $\text{A}/\text{cm}^2$ . With a pumping pulse of 8.0  $\text{A}/\text{cm}^2$  (peak current density with 1.6  $\mu\text{s}$  FWHM), laser action with a low-loss cavity was observed for 1.5  $\mu\text{s}$  but was so close to threshold that the laser energy was only 10 mJ.

The laser experiments were repeated with various output couplings. Figure 3 shows the effect of the coupling on laser power. From Eq. (1), the saturation intensity, gain, and loss were calculated using the data points shown in Figure 3.

$$\frac{I}{I_s} = (1-A) \frac{1-(r)^{1/2}}{1-(1-A)^2(r)^{1/2}} \left\{ g_o L + \ln[(1-A)^2(r)^{1/2}] \right\}. \quad (1)$$

This equation is a modified version of the one given by Rigrod<sup>5</sup> for high-gain lasers. In the derivation here, we have included a lumped loss just in front of each mirror (as an approximation to loss in the laser medium itself) which absorbs a fraction  $A$  of the power incident upon it. Since the laser beam passes each lumped loss twice in a round trip, the single-pass loss represented by each is  $1-(1-A)^2$ . The other symbols have their usual meanings:  $g_0$  is the small-signal gain coefficient,  $L$  is the length of the excitation region,  $r$  is the reflectivity of the output mirror, and  $I_s$  is the saturation intensity. The best fit of the data gave  $g_0 L = 2.0$ ,  $1-(1-A)^2 = 0.5$ , and  $I_s = 0.26$  MW cm<sup>-2</sup>. The value for the single-pass loss is unexpectedly high. However, recent probe measurements suggest that  $F^-$  absorption could account for the high loss.<sup>6</sup>

The principal purpose of this work was to demonstrate long-pulse (cw) operation. Inspection of Figure 2 indicates that even longer laser pulses than 1  $\mu$ s are possible. Note that the laser intensity is increasing as long as the pumping level is above 8.5 A/cm<sup>2</sup>. This implies that longer laser pulses at this pumping level would be more efficient. Also we believe depopulation of the lower level which is bound by 1100 cm<sup>-1</sup><sup>7</sup> and gas heating are not problems at these power levels. In fact the calculated temperature rise of 110°C may enhance the power output by improving the rate of dissociation of the lower level.

The energy deposited in the gas was calculated<sup>8</sup> to be 60 J at

2.5 atm which gives an efficiency of 0.5%. This value is to be compared with the 3% figure reported earlier for short-pulse operation.<sup>3</sup> Much of the difference between these two values is due to the different method of calculating e-beam energy deposition.

Efficiencies  $\sim 1\%$  are of interest for practical devices. We note that the use of a higher-voltage gun allows longer powerful pumping pulses and that greater net efficiency will result.

### References

1. S. K. Searles and G. A. Hart, Appl. Phys. Lett. 27, 243 (1975);  
C. A. Brau and J. J. Ewing, Appl. Phys. Lett. 27, 435 (1975).
2. R. S. Bradford, Jr., W. B. Lacina, E. R. Ault, and M. L. Bhaumik,  
Inter. Quantum Elec. Conf., Amsterdam, 1976, Postdeadline paper  
(unpublished).
3. E. R. Ault, R. S. Bradford, Jr., and M. L. Bhaumik, Appl. Lett.  
27, 413 (1975).
4. J. Jansen, Soc. Photo-Opt. Inst. Eng., 17th Tech. Meeting, San Diego,  
1973 (unpublished).
5. W. W. Rigrod, J. Appl. Phys. 36, 2487 (1965).
6. J. Mangano and J. Jacobs, 3rd Annual Conf. on Electronic State  
Transition Lasers, Aspen, Colo., 1976 (unpublished).
7. J. Tellinghuisen, G. C. Tisone, J. M. Hoffman, and A. K. Hays,  
J. Chem. Phys. 64, 4796 (1976).
8. S. K. Searles and G. A. Hart, Appl. Phys. Lett. 28, 384 (1976).

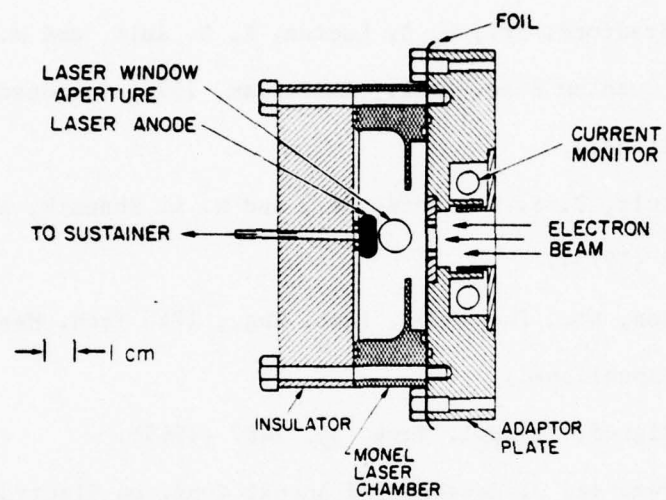


Figure 1. Schematic diagram of the laser cell. The sustainer electrode was grounded in these experiments.

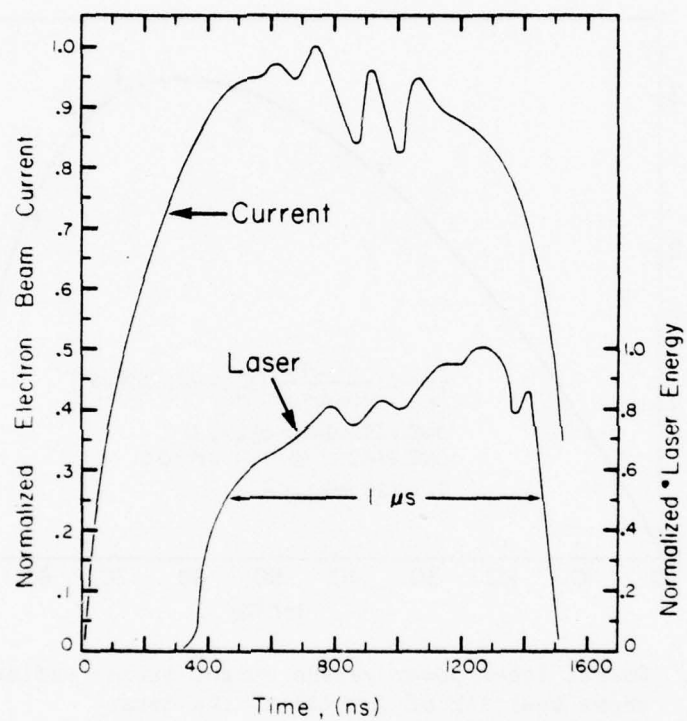


Figure 2. Electron beam current and laser waveforms. Peak current corresponds to  $11 \text{ A/cm}^2$  at the foil. Total pressure 1 atm.

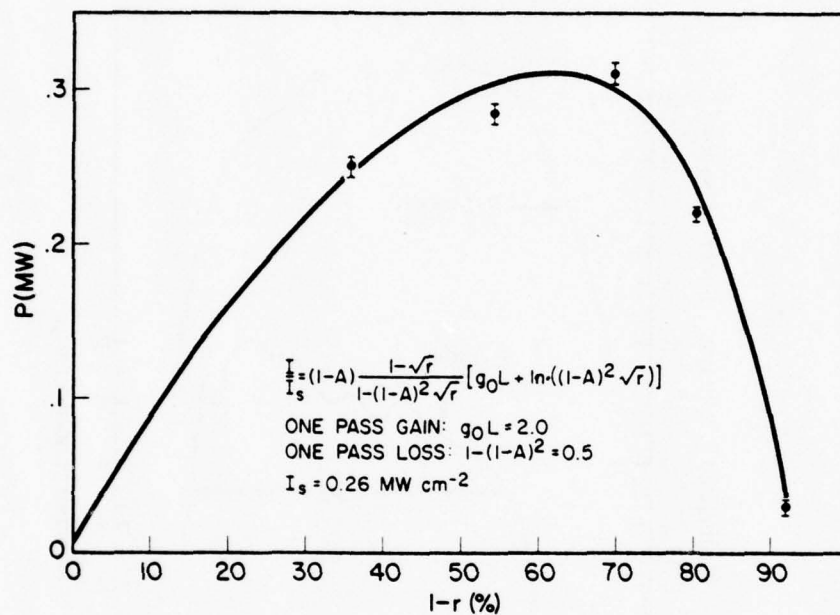


Figure 3. Output laser power versus output mirror reflectance. Line shows best fit of Eq. (1) to the data.

## THE INFLUENCE OF DILUENT GAS ON THE XeF LASER

L. G. Champagne and N. W. Harris  
Naval Research Laboratory, Washington, D. C. 20375

### ABSTRACT

The effect of substituting neon for argon as the diluent gas in electron beam pumped XeF lasers is described. Increased optical extraction energies of  $2.8 \text{ J-l}^{-1}$  and efficiencies of 1.8% are observed. Gain and loss measurements in the laser medium show that the improved performance of the XeF laser in neon diluent is due to a reduction in the loss in the medium.

In a recent paper<sup>1</sup> we reported the long-pulse operation of an electron-beam pumped XeF laser in argon diluent. The analysis of the laser performance indicated that the output power was limited by transient absorption processes occurring during the excitation pulse. This transient absorption, or loss, in rare gas halide lasers, which occurs in both e-beam pumped and e-beam controlled discharges, has been observed elsewhere at several selected wavelengths from 249 nm to 450 nm.<sup>2-6</sup>

In this paper, we report detailed measurements of the extent of these loss processes and of the XeF laser gain and performance in both argon and neon diluents with e-beam pumping. In argon, the laser gain is offset by absorption losses which are more severe at higher input energies. However, in neon diluent, the absorption losses are lower and are observed to be independent of input energy. The replacement of the argon diluent by neon increases the electrical efficiency (energy-extracted/energy-deposited) of the XeF laser at the maximum output from 0.5% to 1.8% and the volumetric output from 0.8 to 2.8 J/l.

The experimental apparatus, which was described previously,<sup>1, 6</sup> has a 1-meter laser chamber equipped with 2.2 cm diameter Brewster-angle windows. Electron beam pulses of 1  $\mu$ sec width and variable intensity up to 10 A/cm<sup>2</sup> were delivered to the gas. A pulsed ion laser similar to that described by Simmons and Witte<sup>7</sup> was used to probe the discharge. An argon ion line at 364 nm and a neon ion line at 338 nm<sup>8</sup> were used to measure the loss on either side of line center. A prism was placed at the output of the probe laser to select the required probe wavelength.

On-line gain was measured using a discharge pumped<sup>9</sup> XeF laser as well as an argon-ion line at 351.1 nm. The gain measured by the XeF laser was 30% greater than that measured by the argon ion laser. This higher value for the gain is thought to be more representative of the gain on line center for the e-beam pumped XeF laser and is reported below.

The probe pulse was monitored by S5 photodiodes before and after the laser chamber. A long optical path length between the chamber and the output diode was used to reduce the fluorescence signal to less than 10% of the laser signal.

Figure 1 shows the gain and loss measurements of the XeF laser at the optimum operating pressure (2.5 atmospheres) and gas composition (Ar:Xe:NF<sub>3</sub>::99.5:0.36:0.12) for argon diluent gas at maximum output power. These measurements are plotted against the energy deposited by the electron beam as calculated by the method used in Ref. 10. Two gain curves are plotted, gain as measured and the zero loss gain (medium gain corrected for loss). The loss measurements on either side of line center were the same within experimental error. The loss in pure argon was also measured (at 351.1 nm) and is seen to be much greater than the loss of the laser gas mixture.

Figure 2 shows the comparable measurements for neon diluent gas. In this case the composition was Ne:Xe:NF<sub>3</sub>::99.75:0.18:0.06 at a pressure of 5 atmospheres. Thus the same beam energy was deposited in argon and in neon for equal electron beam currents. From these results it is clear that the loss is caused by the diluent gas and that similar losses are

produced when pure argon or neon is irradiated. In the presence of the other laser gas constituents the loss is reduced but while it is essentially eliminated in the neon diluent case there is still a significant loss in argon diluent. These data indicate the existence of collisional processes which either remove the absorbing species or prevent its formation.

A plausible explanation for the difference between argon and neon is that Penning ionization can occur in neon. The neon metastable atom has sufficient energy to ionize the xenon atom whereas the argon metastable atom is not sufficiently energetic. Experiments designed to identify the absorbing species are underway.

Figure 3 shows the variation in output power as a function of mirror coupling for both argon and neon diluent. Other conditions are as for Figs. 1 and 2, with the energy input kept constant at 158 J/l. With the gain the loss data described above the saturation intensity was calculated using the method of Ref. 1. This gives a saturation intensity of  $0.32 \text{ MW/cm}^2$  for argon diluent and  $0.37 \text{ MW/cm}^2$  for neon diluent. These values agree within the experimental uncertainties, thus providing additional indication that the difference in laser performance between the diluents can be attributed to changes in the loss processes rather than to the gain processes.

The most striking difference between the two diluents is seen in Fig. 4 where efficiency is shown as a function of pressure. The efficiency attained with neon rises with pressure up to the limit of the

apparatus (5 atmospheres) whereas the efficiency using argon falls. For the argon diluent the output mirror coupling was optimized at each pressure to take account of the change in loss with pressure. The loss in neon is small and constant and hence the optimum coupling did not change with pressure. When neon is used as the diluent, the gas composition is not kept constant but is optimized at each operating pressure. It was found that the maximum output power was obtained with constant number densities of  $6 \times 10^{16}/\text{cm}^3$  for  $\text{NF}_3$  and  $1.8 \times 10^{17}/\text{cm}^3$  for Xe. The output power was much more sensitive to the number density of  $\text{NF}_3$  and Xe for the neon diluent than for the argon diluent. The maximum output energy from this laser using argon diluent was 0.31 J at a pressure of 2.5 atmospheres which corresponds to an efficiency of 0.5%. Using neon diluent the maximum energy measured was 1.08 J with an efficiency of 1.8% at a pressure of 5 atmospheres. The active volume is 0.38 liter.

#### Conclusions

We have demonstrated much improved efficiency (1.8%) and optical energy extraction ( $2.85 \text{ J-l}^{-1}$ ) by substituting neon for argon as the diluent in the XeF laser. The improvement is shown to be due to a reduction in the loss in the medium. Work presently in progress includes identifying the details of the loss mechanism and investigating the effect of diluent gas on an electron beam controlled discharge XeF laser.

#### Acknowledgment

The authors are grateful for the technical assistance rendered by D. M. Shores and R. DeLoatch.

### References

1. L. F. Champagne, J. G. Eden, N. W. Harris, N. Djeu and S. K. Searles, Appl. Phys. Lett. 30, 160 (1977).
2. R. O. Hunter, C. Houton, J. Oldnettel, Post deadline paper, Third Summer Colloquium on Electronic Transition Lasers, Snowmass, CO., September, 1976.
3. E. Zamir, D. L. Heustis, D. C. Lorents and H. H. Nakano, Third Summer Colloquium on Electronic Transition Lasers, Snowmass, CO., September, 1976.
4. H. T. Powell and J. R. Murray, Lawrence Livermore Laboratories Laser Program Annual Report - 1974, (March 1975).
5. J. A. Mangano and J. H. Jacobs, Private communication.
6. L. F. Champagne, J. G. Eden, N. W. Harris and S. K. Searles, Proceedings Third Summer Colloquium on Electronic Transition Lasers, Snowmass, CO., September 1976.
7. W. W. Simmons and R. S. Witte, IEEE J. Quantum. Electron. QE-6, 648 October 1970.
8. W. B. Bridges and A. N. Chester, Applied Optics 4, 573 (1965).
9. R. Burnham and N. Djeu, Appl. Phys. Lett. 29, 709 (1976).
10. S. K. Searles and G. A. Hart, Appl. Phys. Lett. 28, 384 (1976).

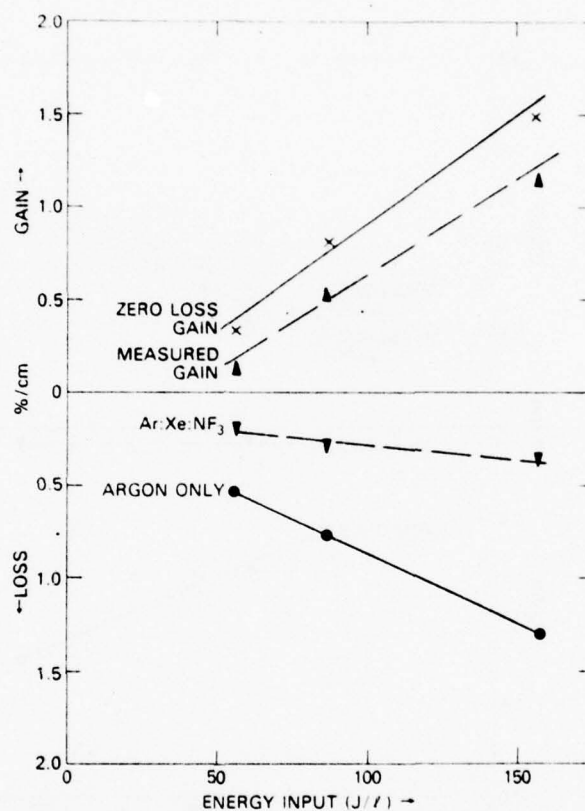


Figure 1. Measured gain at 351.1 nm and loss at 338 nm and 364 nm in Xef laser mixtures as a function of deposited energy for argon diluent.

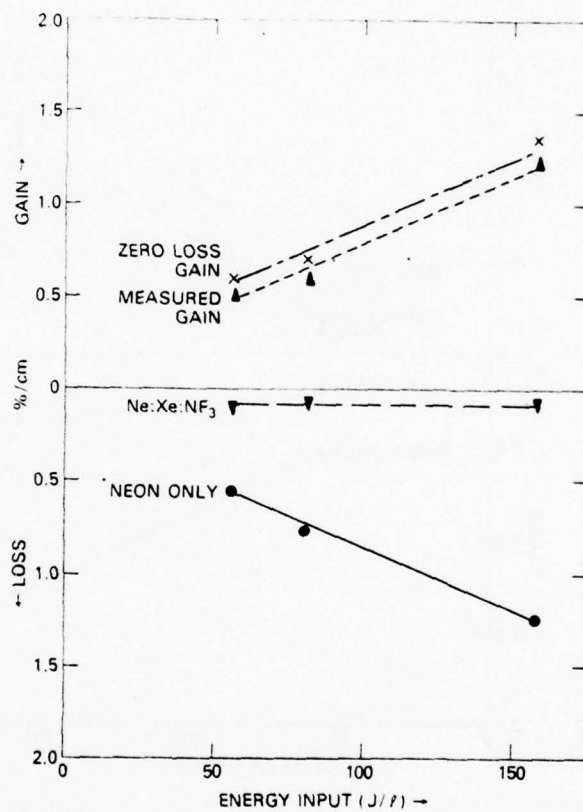


Figure 2. Gain and loss measurement as a function of deposited energy for neon diluent.

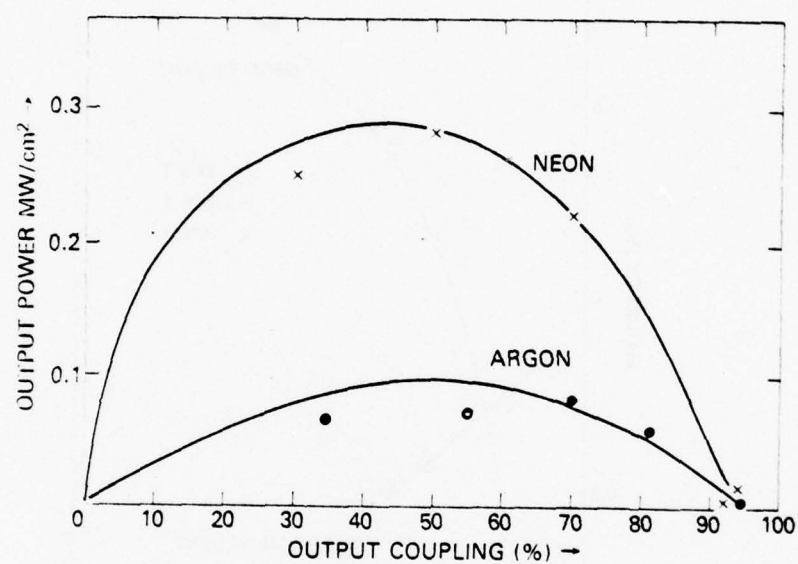


Figure 3. XeF laser output power as a function of output coupling for neon and argon diluents.

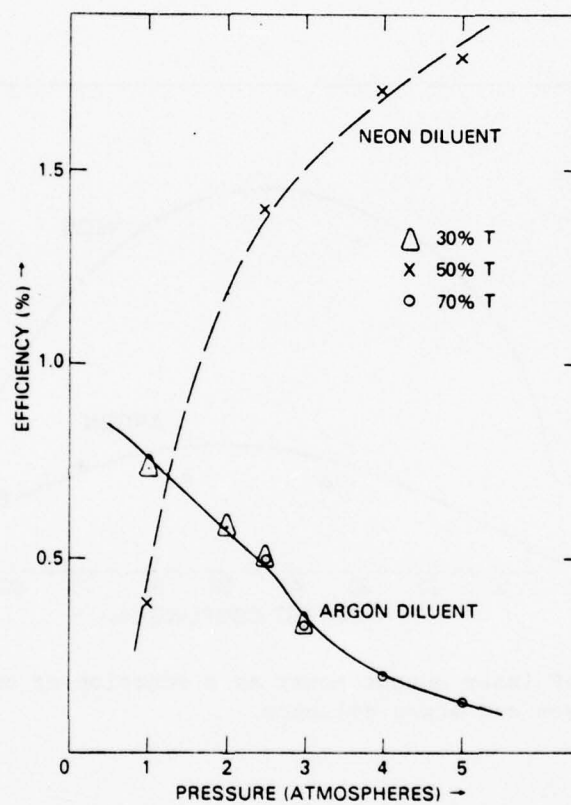


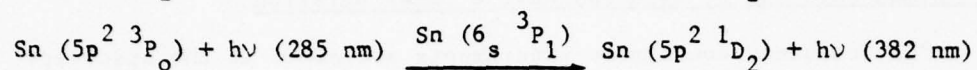
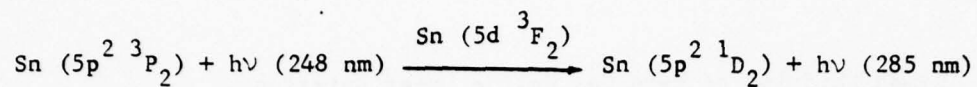
Figure 4. Efficiency of XeF laser as a function of total pressure for neon and argon diluents.

#### 4. Raman Shifting of Rare Gas Halide Laser Emission

The frequency conversion experiments are aimed at the discovery of efficient means of shifting the KrF laser wavelength to a region for which propagation losses would be acceptable. The approach taken at NRL is based on stimulated resonant Raman scattering in metal vapor systems. This method has in the past been shown to be extremely efficient in shifting visible and near-u.v. radiation into the infrared. It seems to be well suited for the present objective both because of the high gain of the process and the magnitude of the frequency shift it affords.

In a prototype experiment we have successfully shifted the XeF laser output at 351 nm to 585 nm in Ba vapor. Photon conversion efficiency as high as 90% was achieved in that experiment. The Raman output was obtained in one-pass superradiance, and the spatial profile of the Raman beam was of a high quality. Details of this work may be found in the following reprint [Efficient Raman Conversion of XeF Laser Output in Ba Vapor].

For the conversion of the KrF laser output, two similar resonant Raman schemes are possible. They would employ Sn vapor and Ca vapor, with expected output at 382 nm and 545 nm respectively. In the scheme using Sn as the Raman medium, two successive resonant Raman scattering processes are required, with the first one yielding an output at 285 nm. The energy levels involved are as follows:



where the states written above the arrows are the resonant intermediate states. Thus far, we have observed in preliminary experiments stimulated emission at 285 nm at Sn densities substantially below the required  $10^{16} \text{ cm}^{-3}$ . Work on this system will be resumed shortly when an improved Sn oven becomes available.

EFFICIENT RAMAN CONVERSION OF  
XeF LASER OUTPUT IN Ba VAPOR\*

N. Djeu and R. Burnham<sup>†</sup>

Naval Research Laboratory  
Washington, D. C. 20375

ABSTRACT

Intense Raman emission at 585 nm has been observed from Ba vapor pumped by the XeF laser. Near unit photon conversion efficiency was measured.

\* Work supported by the Defense Advanced Research Projects Agency under Order No. 2062

<sup>†</sup> Science Applications, Inc., Arlington, VA

Within the last year or so a number of rare gas halide lasers have been made with either e-beam excitation<sup>1-3</sup> or discharge pumping,<sup>4</sup> or a combination of both.<sup>5</sup> The high efficiency of these lasers has made them prime candidates for a variety of potential applications. For some of these applications, efficient means of shifting the rare gas halide laser output to other wavelength regions must first be found. We wish to report here the near unit photon conversion of the XeF laser output at 351 nm to 585 nm in Ba vapor. This is the first demonstration of an efficient wavelength conversion scheme for the rare gas halide lasers.

Stimulated Raman scattering in atomic vapors was first observed by Sorokin et al.<sup>6</sup> and Rokni and Yatsiv.<sup>7</sup> More recently, the resonant Raman effect has been applied to the generation of tunable infrared radiation by several groups.<sup>8,9</sup> Electronic Raman scattering as a means of wavelength conversion is particularly well suited for the rare gas halide lasers. The near UV wavelengths of these lasers are nearly resonant with a number of highly allowed atomic transitions whose upper states are connected just as strongly to some low lying excited states, making the gain for these corresponding Raman transitions extremely large even for modest pump power densities. For near-resonant Raman scattering, the three level approximation is valid, and the Raman gain coefficient is given in MKS units by

$$\alpha_R = \frac{e^4 f_1 f_2 \nu_R n I}{32 \pi^3 \epsilon_0^2 m^2 h c^2 \nu_1 \nu_2 \Delta \nu^2 \gamma}$$

Here  $f_1$  and  $f_2$  are the  $f$ -values for the two connected transitions,

$\nu_1$  and  $\nu_2$  the corresponding frequencies,  $\nu_R$  is the Raman frequency,  $\Delta \nu$  the resonance defect,  $n$  the density of population difference between the initial and final states,  $I$  the intensity of the pump beam, and  $\gamma$  the sum of dephasing rates for the initial and final states. It is assumed that the levels are homogeneously broadened, and the linewidth of the pump laser  $\Gamma$  is much smaller than  $\gamma$ . For  $\gamma \lesssim \Gamma \ll \Delta \nu$ , the formula is approximately valid if  $\Gamma$  is used instead of  $\gamma$ . In a typical case for the rare gas halide lasers,  $\Gamma = 10^{11} \text{ sec}^{-1}$  and  $I = 10^{13} \text{ W m}^{-2}$  at the waist of a focused beam. Therefore, for  $f_1 = f_2 = 0.1$ ,  $n = 10^{23} \text{ m}^{-3}$ , and a pump frequency of  $10^{15} \text{ sec}^{-1}$ , one can be as far off resonance as  $4 \times 10^{13} \text{ sec}^{-1}$  ( $1300 \text{ cm}^{-1}$ ) and still have a gain of  $10 \text{ m}^{-1}$  at the Raman wavelength. In the present experiment on the Ba conversion of the XeF laser output, the relevant energy levels for which are shown in Fig. 1, the pump photons are approximately  $75 \text{ cm}^{-1}$  from resonance with the intermediate state.

A diagram of the overall experimental configuration is given in Fig. 2. The basic XeF discharge laser has been described earlier.<sup>4</sup> However, for the Raman conversion work here, additional elements have been included to improve the beam quality. The cavity consisted of a  $1800 \text{ line nm}^{-1}$  grating and a 30% reflecting 3 m radius of curvature output mirror separated by 1.35 m. A 0.89 mm diameter pinhole placed in front of the output mirror produced a beam in the fundamental transverse mode. The use of 5 quartz plates inside the cavity in addition to the two windows, all oriented at Brewster's angle, forced the output to be linearly polarized. The grating selected the group of "lines"

near 351 nm out of the possible three in XeF which would normally be observed in the absence of any wavelength discrimination.<sup>4</sup> The resulting output contained three "lines" separated by approximately  $10\text{ cm}^{-1}$  and  $15\text{ cm}^{-1}$ , with the larger gap lying towards longer wavelength. The width of each "line", as determined from densitometer tracings of spectral records, was no greater than the spectrograph instrument width of  $2\text{ cm}^{-1}$ . Typical output power and energy of this laser were 1 kW and 25  $\mu\text{J}$ .

The output from the XeF laser was partially reflected by a quartz plate onto a reference photodiode  $D_1$ , and then focused into the Ba heat pipe oven by a 30 cm focusing lens. The 25 mm diameter heat pipe and its wick were made from stainless steel tubing of 1.5 mm wall thickness and screen of 120 mesh in a way similar to that described by Vidal and Cooper.<sup>10</sup> The oven had a heated zone of 40 cm and could be operated up to  $1200^\circ\text{C}$ . The beam emerging from the Ba heat pipe was split again for simultaneous measurements by either two photodiodes or one photodiode ( $D_2$ ) and one joulemeter ( $D_3$ ) depending on what quantities were to be correlated.

Raman emission became evident at an oven temperature of about  $1000^\circ\text{C}$ , before the heat pipe mode of operation was established. The Raman output had a divergence comparable to that of the pump beam, and contained polarizations both parallel and perpendicular to that of the pump. Replacing the 30 cm focusing lens by either a 20 cm or a 50 cm focusing lens reduced the extent of Raman conversion. Spectrographic records of the Raman output showed three "lines" near 585.0 nm as expected. The widths of the components again appeared to be no greater than that of the spectrograph.

The relationship between the Raman pulse and the transmitted pump pulse was first examined. For that purpose, appropriate UV and orange bandpass filters were used for  $F_2$  and  $F_3$  (with  $F_1$  left out), and photodiode detectors for  $D_2$  and  $D_3$ . The simultaneous oscilloscope traces for the Raman and transmitted pump pulses are shown in Fig. 3(b), together with the input reference pulse as monitored by  $D_1$  in Fig. 3(a). Here the transmitted pump pulse should be reduced somewhat for a direct comparison with the input reference, and the displacement in time between the two pictures resulted from the use of different triggering modes. Transmitted pump pulses with even smaller areas have been observed in other runs. But regardless of its magnitude as the Ba vapor pressure was varied, it always retained the double peak feature shown in Fig. 3(a), with the right hand peak considerably higher than the one to the left. This indicated that the gain for the same pump intensity was lower towards the end of the pulse than the beginning. Since the effective interaction length for the focused beam was only on the order of a few centimeters, it was thought that perhaps depletion of ground state atoms might have been responsible. Although a rough calculation corroborated this hypothesis, studies of the amplitude of the right hand peak as a function of pump pulse energy at fixed Ba pressure failed to confirm it. Another likely cause that came to mind was that the three "lines" in the XeF laser output did not have the same temporal behavior, with the one farthest from resonance coming out latest in time. Comparison of the individual frequency resolved components with an undispersed reference showed that the "lines" were indeed staggered in such a

sequence. Whether additional factors might have been contributing towards the observed gain symmetry is unclear at present.

The efficiency of the Raman conversion process was measured as follows. Referring again to Fig. 2, the filters  $F_2$  and  $F_3$  were now removed, and a joulemeter was used instead of the photodiode for  $D_3$ . With the Ba oven unheated and no filters at all, the photodiodes  $D_1$  and  $D_2$  were first calibrated against the joulemeter  $D_3$ . Then at the maximum Ba pressure of 10 torr, the output from the heat pipe, after passage through an orange bandpass filter with known transmission at 585 nm, was monitored again by  $D_2$  and  $D_3$ . Since the beam-splitting quartz plate for the output was tilted from the optical axis by only  $10^\circ$ , it had nearly the same reflectivity for both polarizations of the Raman pulse. Photodiode  $D_2$  was again calibrated with respect to the joulemeter, this time at 585 nm. A comparison of the input XeF laser pulse monitored by  $D_1$  with the Raman pulse monitored by  $D_2$  then gave the efficiency of the conversion process. For the maximum intensity obtainable from our XeF laser ( $40 \text{ MW cm}^{-2}$  in the focal region), the photon conversion efficiency was measured to be 80% for the entire pulse and greater than 90% at the peak of the pulse. As an independent check on the accuracy of the measurements, the photodiode  $D_2$  was calibrated using the 351 nm line from the CW Ar ion laser and a CW dye laser output at 585 nm. The beams were chopped at a very low duty cycle ( $\sim 10^{-3}$ ) in order to avoid any detector saturation. The relative sensitivity of  $D_2$  at the two wavelengths determined from this procedure was in excellent agreement with that determined earlier.

It should be noted that the extremely high conversion efficiency observed in the present experiment was achieved without a cavity for the Raman medium. In addition, we have used a pinhole for transverse mode selection of the pump laser which severely limited its output intensity. The pump power density can be greatly increased by either employing an unstable resonator or amplifying the beam after expansion. Together with the use of a mode matched cavity for the Raman medium, one can expect efficient rare gas halide laser output conversion in much less favorable resonant Raman systems.

### References

1. J. J. Ewing and C. A. Brau, Appl. Phys. Lett. 27, 350 (1975).
2. C. A. Brau and J. J. Ewing, Appl. Phys. Lett. 27, 435 (1975).
3. J. M. Hoffman, A. K. Hays, and G. C. Tisone, Appl. Phys. Lett. 28, 538 (1976).
4. R. Burnham and N. Djeu, Appl. Phys. Lett. 29, 707 (1976).
5. J. A. Mangano and J. H. Jacob, Appl. Phys. Lett. 27, 495 (1975).
6. P. O. Sorokin, N. S. Siren, J. R. Lankard, E. C. Hammond, and T. G. Kazyaka, Appl. Phys. Lett. 10, 44 (1967).
7. M. Rokni and S. Yatsiv, Phys. Lett. 24A, 277 (1967).
8. J. L. Carlsten and P. C. Dunn, Opt. Commun. 14, 8 (1975).
9. A. Cotter, D. C. Hanna and R. Wyatt, Opt. Commun. 16, 256 (1976).
10. C. R. Vidal and J. Cooper, J. Appl. Phys. 40, 3370 (1969).

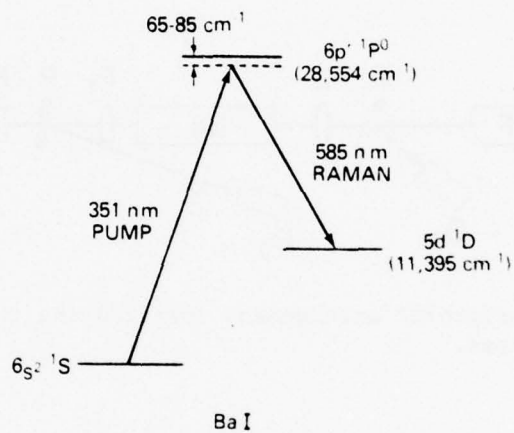


Figure 1. Energy levels in Ba relevant to the Raman shifting of XeF laser wavelength.

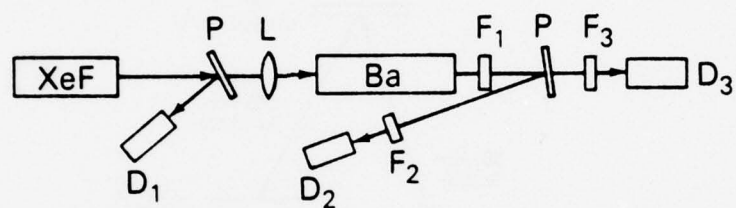


Figure 2. Experimental arrangement for studying the Raman conversion process.

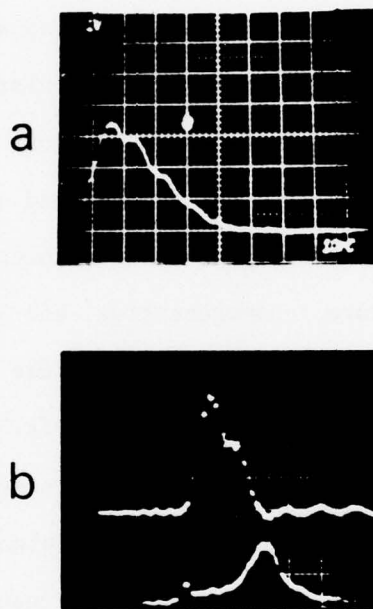


Figure 3. Simultaneously detected input XeF laser pulse (a), Raman output (top trace in b) and transmitted portion of input (bottom trace in b). Both pictures taken with 10 nsec/div. timescale.

## 5. Progress in New Lasers with the NRL 50 ns Electron Beam Apparatus.

### E-Beam Initiated Lasers

#### Introduction

NRL's Laser Physics Branch is conducting an intensive study of prospective visible and uv atomic and molecular laser systems. The metal vapor excimer molecules offer tremendous potential as tunable, high energy storage lasers in the visible and uv portions of the spectrum. To date, however, technological problems (handling of the metal vapor, temperature inhomogeneities, etc.) have thwarted the exploitation of the unique properties of these molecules. In this section, our efforts to develop efficient visible and ultraviolet lasers using the group I and IIB. metals are described. Considerable success in the design of high temperature, high pressure e-beam cells as well as demonstration of lasing on the green band of HgCl are reported.

#### Electron Beam Machine Modifications

In our last report, the design, construction and initial testing of a new high temperature electron beam cell was discussed. The most difficult problem facing us at that time was low foil lifetime ( $< 10$  shots at high temperature. It was determined that this problem was due to absorption in the foil of low energy electrons (stored in the Blumlein) that arrived at the foil after the termination of the main 50 ns pulse. To circumvent this problem, a diverter switch (shown in Figure D) was designed and installed in the final section

of the Blumlein may be short-circuited at any time following the main pulse. Since the switch's installation, the lifetime of the Inconel 718 foil has not been reached. The limiting factor on the "up" time for the high temperature e-beam cell is now temperature cycling of the vacuum gaskets. In any case, the diverter switch installation has reduced our foil lifetime problems.

In February, the LC generator and 8  $\Omega$  Blumlein were also completely overhauled. All switches were refitted and "heater" capacitors were installed in the LC generator to decrease the units charging risetime. As a result, the machine's beam current, for a fixed diode gap, was quadrupled.

#### Heated Cell Improvements

Several improvements in the design of the heated e-beam cell (shown schematically in Figure E) have resulted in:

- a) Lower turbulence of the gaseous laser medium and
- b) elimination of window fogging and foil condensation problems.

Optical quality sapphire windows were installed normal to the laser cell's axis using gold gaskets. Heating tape kept the window's temperature  $\sim 25^{\circ}$  hotter than the cell. All swagelok fittings were replaced by Varian 1 3/4" o.d. flanges and copper gaskets for better vacuum integrity. A high temperature stainless-steel valve was placed in the metal reservoir line and the cell temperature was maintained  $25-50^{\circ}$  C higher than the reservoir using heating tapes. As a result, the cell can presently operate up to  $\sim 500^{\circ}$  C with little medium

turbulence.

### Alkali-Rare Gas Studies

#### a. Theoretical

To predict the conditions necessary for obtaining stimulated emission on the A $\rightarrow$ X and C $\rightarrow$ X bands of the alkali-rare gas diatomic molecule, and simple kinetics model of e-beam pumped alkali-rare gas mixtures has been constructed. The model, which is described in detail in the following abstract, predicts for NaXe that (see Figure F):

a) NaXe<sup>\*</sup> population of  $\sim 3 \cdot 10^{15} \text{ cm}^{-3}$  are attainable in our device and

b) depletion of the Na(3<sup>2</sup>S) ground state is large, >50%.

These calculations, then, strongly suggest that lasing on the A, C $\rightarrow$ X continua of NaXe (and possibly other alkali-rare gas visible bands) ought to be attainable utilizing our e-beam gun.

#### b. Experimental

Preliminary emission and absorption experiments in alkali-argon (or Xenon) mixtures have been conducted. The goals for this past reporting period were:

1) to obtain a uniform, non-turbulent alkali-rare gas mixture (free from nucleation "droplets") in the electron beam cell and 2) observe alkali atomic emission using direct electron impact and electronic excitation transfer pumping of the alkali.

Cesium was studied initially due to its high vapor pressure

and the resulting ease of handling. For Cs/Ar mixtures of [Cs]  $10^{16} \text{ cm}^{-3}$  and [Ar]  $\sim 10^{20} \text{ cm}^{-3}$ , atomic Cs emission of the sharp ( $n^2s \rightarrow 6^2p$ ) and diffuse series ( $n^2d \rightarrow 6^2p$ ) was observed. An attempt to enhance this fluorescence using the kinetic sequence:

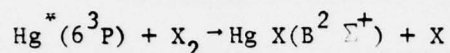
$\text{Ar}^M \rightarrow \text{N}_2^* (\text{A}^3\Sigma) \rightarrow \text{Cs}^*$  was not successful. Further study to clarify the reasons for this is necessary. Similar experiments were conducted on K/Ar mixtures and, again, weak  $\text{K}^*$  fluorescence was observed. Absorption spectra of K/Xe high pressure mixtures ([K]  $\sim 10^{16} \text{ cm}^{-3}$ , [Xe]  $\sim 10^{20} \text{ cm}^{-3}$ ) reveal strong KXe ( $X \rightarrow C$ ) absorption of 560 nm as shown in Figure G. This is probably due to a ground KXe ( $^2\Sigma$ ) state that is weakly repulsive ( $\leq 400 \text{ cm}^{-1}$ ) at  $R_e$  for the KXe( $C^2\Sigma$ ) level. This problem, however, does not exist for NaXe( $C^2\Sigma$ ) (see Figure H). Broad-band absorption measurements failed to reveal any  $X \rightarrow C$  absorption. Also, optical pumping of the NaXe C state using XeF and  $\text{N}_2$  lasers has yielded the blue  $C \rightarrow X$  radiation. In spite of the long  $C \rightarrow X$  radiative lifetime,  $\sim 1\text{-}5 \text{ }\mu\text{s}$ , the 440 nm band intensity obtained makes NaXe( $C \rightarrow X$ ) a promising blue laser candidate. Electron beam pumping of this molecule will be attempted shortly using Ar/Xe/Na gas mixtures.

#### Mercury Halide Experiments

The mercury halide molecules offer many of the attractive qualities of the rare gas-halide family and yet lase in the visible. Therefore, these lasers are ideal for DARPA applications.

What makes these lasers so attractive is the efficiency with which  $\text{Hg}^* (6^3\text{P})$  metastables may be created in a low pressure ( $\leq 1 \text{ atm}$ )

discharge or high pressure (105 atm) e-beam excited plasmas. Also since  $\text{Hg}^* (6^3\text{P})$  has chemical properties similar to the rare gas ( $^3\text{P}$ ) metastables, then reaction of  $\text{Hg}(6^3\text{P})$  with halogen bearing molecules via the "harpoon" process:



is extremely efficient.

We have observed stimulated emission on the  $\text{B} \rightarrow \text{X}$  band of  $\text{HgCl}$  utilizing e-beam excitation of  $\text{Ar/Xe/Hg/CCl}_4$  mixtures.

As can be seen from Figure I,  $\text{HgCl}$  lases on 2 lines, 576.6 and 583 nm, which are attributed to  $v=0 \rightarrow v'=22$  transitions on the  $\text{B} \rightarrow \text{X}$  band of  $\text{HgCl}^{37}$  and  $\text{HgCl}^{35}$ , respectively. Although output energies of 1 mJ have been obtained, it is likely that energy densities of several joules/liter can be obtained using higher output coupling.

A preprint of a publication of the  $\text{HgCl}$  laser follows.

The demonstration of efficient, line tunable oscillation in the blue-green from the  $\text{HgX}$  family ( $\text{X}=\text{Cl}, \text{Br}$  and  $\text{I}$ ) will be the subject of intensive research at NRL in the next several months. The logical extension of this research to the  $\text{CdX}$ , and possibly  $\text{ZnX}$ , molecules is anticipated.

#### Conclusion

In summary, we have been successful in developing some of the technology necessary to investigate various metal excimer lasers which require high temperature environments. The promising characteristics of these molecules as efficient lasers in the visible make them

attractive areas for future research.

Electron Beam Excitation of Sodium-Xenon Gas Mixtures - Abstract\*

Initial experimental and theoretical studies to determine the feasibility of obtaining stimulated emission on the A, C-X bands of NaXe have been performed. To predict the operating conditions necessary for lasing, the following model of electron beam-pumped Na-Xe mixtures has been developed. A monoenergetic 433 KeV beam of electrons (beam energy = 100 J), after penetrating a 1 mil foil, excites a high pressure mixture of Sodium and Xenon,  $[Na] \sim 4 \cdot 10^{16} \text{ cm}^{-3}$  and  $[Xe] \sim 10^{20} \text{ cm}^{-3}$ . The beam energy is absorbed by the Xe through the collisional process: (1)  $\vec{e} + Xe \rightarrow Xe^+ + e_7 + \vec{e}$  where  $\vec{e}$  and  $e_7$  represent high energy ( $\leq 433 \text{ KeV}$ ) and 7 eV electrons, respectively.<sup>1</sup> The e-beam current pulse is approximated by a trapezoid with rise and fall times of  $\sim 14 \text{ ns}$ . The central portion of the waveform has a halfwidth of 36 ns and rises at 165 A/ns.

Excitation of the  $Na^*$  ( $3^2P$  or  $4^2S$ ) levels occurs by direct electron impact: (2)  $e_7 + Na \rightarrow Na^* + e_5$ . The excited Sodium atom subsequently radiates to the ground state or forms a  $NaXe^*$  excimer due to teratomic recombination: (3)  $Na^* + 2Xe \rightarrow NaXe^* (A^2\pi \text{ or } C^2\Sigma) + Xe$ . For this model, the formation and dissociation rates of  $NaXe^*$  as measured by Scheps and Gallagher<sup>2</sup> have been used.

Finally, recombination of the  $Xe_2^+$  dimer ion with low energy electrons accounts for the decay of the electron density. Thus, the xenon enters the model only as a perturber in (3) and as a source and

sink of low energy electrons.

Figure F displays the results obtained for the conditions given earlier. Strong depletion of the Na ground state and the high NaXe<sup>\*</sup> population densities obtained point out the attractiveness of Na-Xe plasmas as potential visible lasers. It must be noted, however, that the addition to the model of Na<sup>\*</sup>-Na<sup>\*</sup> collisions and superelastic destruction of Na<sup>\*</sup> (reverse of (2)) will significantly decrease the Na ground state depletion.

Preliminary absorption and e-beam excitation emission studies of the NaXe ( $X^2\Sigma \rightarrow A^2\Pi$ ,  $C^2\Sigma$ ) continua will be described. Absorption of Na-Xe mixtures at 440 nm (corresponding to the peak of the  $X^2\Sigma \rightarrow C^2\Sigma$  band) was determined to be <1%, indicating that small population inversions will be required to observe net gain on the C $\rightarrow$ X blue band of NaXe<sup>\*</sup>.

#### References

1. L. R. Peterson and J. E. Allen, J. Chem. Phys. 56, 6068 (1972)
2. R. Scheps and A. Gallagher, J. Chem. Phys. 65, (1976)

\* Presented at Third Conf. on Chemical and Molecular Lasers, St. Louis, April, 1977.

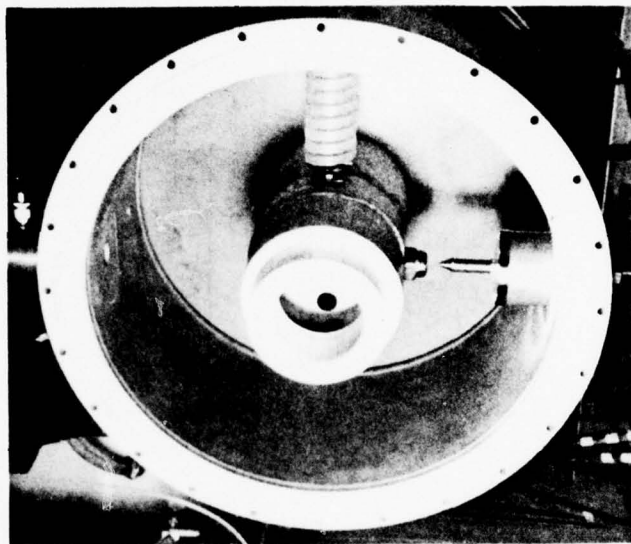


Figure D. Diverter switch with adjustable gap. The switch shorts the center conductor to the outer conductor of the Blumlein after the main pulse.

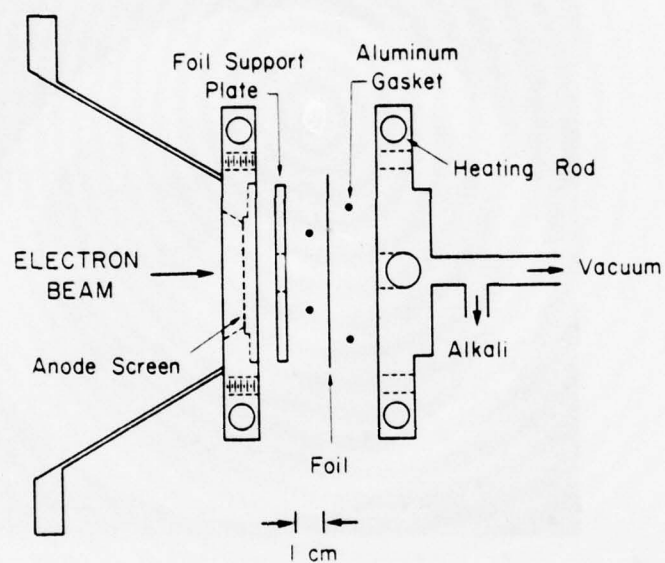


Figure E. Schematic of heated cell fitted to the 50 ns e-beam gun.

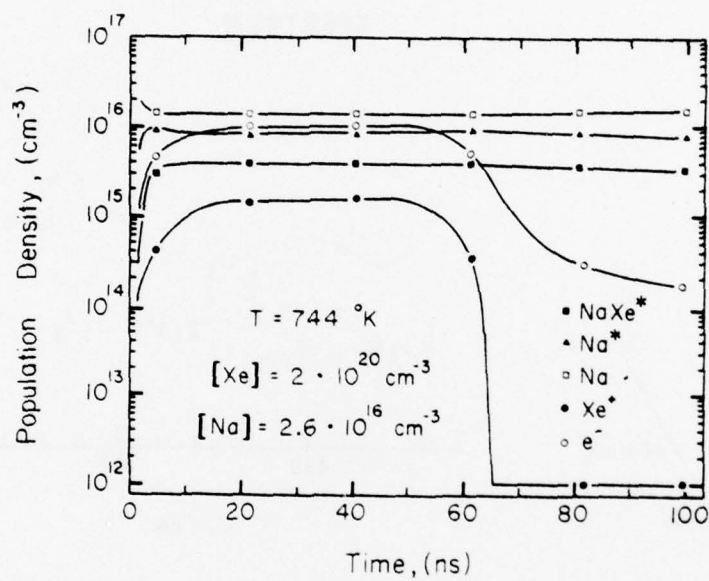


Figure F. Theoretical curves resulting from excitation of Na/Xe mixtures by the NRL gun.

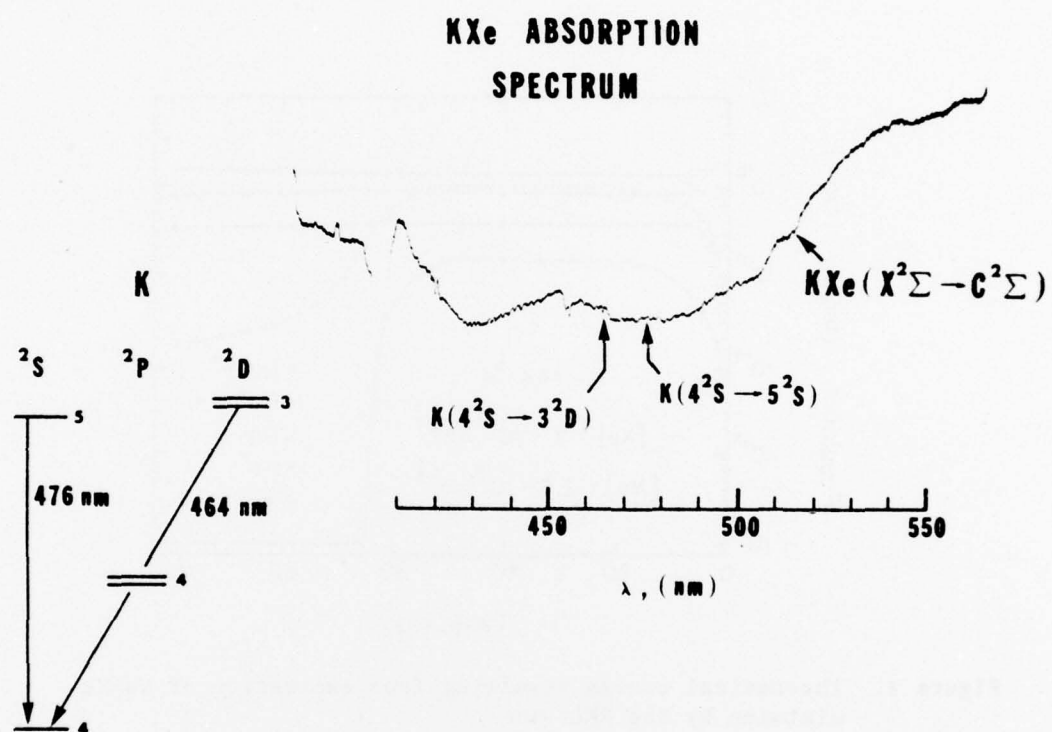


Figure G. Absorption spectrum of an unexcited K-Xe mixture.

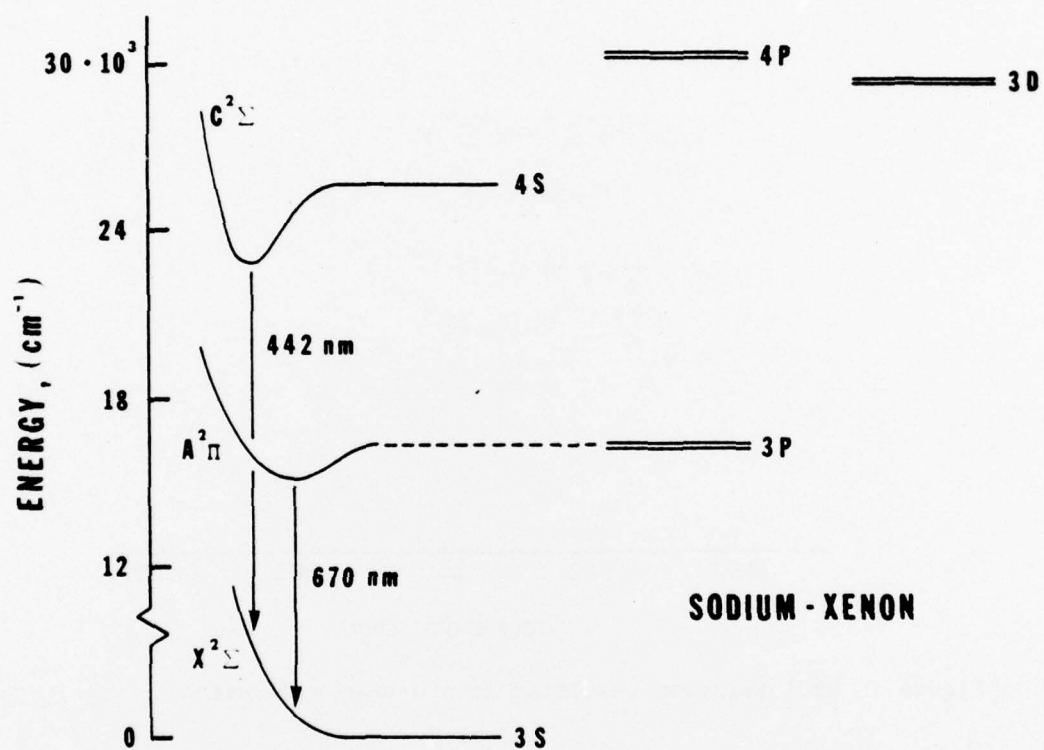


Figure H. Potential excimer laser transitions arising from excited NaXe molecules.

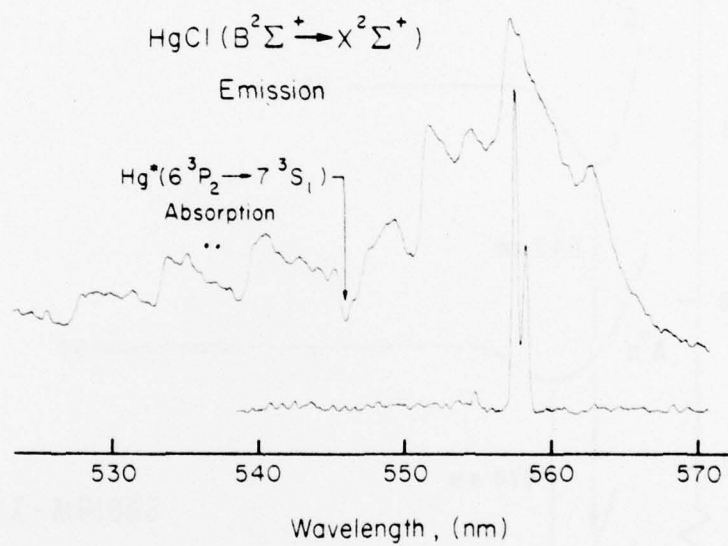


Figure I HgCl emission resulting from e-beam excitation.

GREEN HgCl ( $B^2\Sigma^+ \rightarrow X^2\Sigma^+$ ) LASER\*

J. Gary Eden

Laser Physics Branch,  
Optical Sciences Division,  
Naval Research Laboratory,  
Washington, D. C. 20375

Abstract

Lasing action on the  $v=0 \rightarrow v'=22$  transition of the  $B^2\Sigma^+ \rightarrow X^2\Sigma^+$  band of HgCl has been observed. Electron beam excitation of Ar/Xe/Hg/ $CCl_4$  mixtures produced oscillation at 557.62 and 558.35 ( $\pm 0.15$ ) nm. The mercury-halide family appears promising as an efficient source of line-tunable stimulated emission in the blue-green region of the spectrum.

\* Work supported in part by DARPA

The need for efficient, energetic lasers in the near uv  $\rightarrow$  visible spectral region has recently led to the discovery and development of the rare gas-halide lasers.<sup>1-3</sup> The success of these devices is largely due to the efficiency with which rare gas  $^3P$  metastables are created in low pressure ( $\leq 1$  atm) electric discharges or high pressure (2-5 atm) electron beam pumped systems. Unfortunately, the ultraviolet wavelengths of the rare gas-halide lasers are unsuitable for many applications and so UV-to-visible conversion schemes are sometimes necessary.<sup>4</sup>

The mercury-halide molecules are attractive candidates as visible lasers offering efficiencies comparable to the rare gas-halides. As is the case for the rare gas  $^3P$  metastables, the chemistry of  $Hg^*(6^3P)$  is similar to the alkalis. For example, the ionization potential of  $Hg^*(^3P_2)$  (4.97 eV) is similar to that of  $Na(3^2S)$  (5.14 eV); moreover, the  $6^3P$  states of mercury are known<sup>5</sup> to react with halogen containing molecules via the "harpoon" process<sup>6</sup> used to describe alkali-halide ground state formation. Therefore, several of the features that have made the rare gas-halide excimers so interesting as high power lasers are also characteristic of the mercury-halide molecules.

The observation of stimulated emission on the  $v=0 \rightarrow v'=22$  transition of the  $B^2\Sigma^+ \rightarrow X^2\Sigma^+$  band of  $HgCl$  is described in this paper. Utilizing electron beam excitation of  $Ar/Xe/Hg/CCl_4$  mixtures, double line laser oscillation occurred at 557.62 and 558.35 ( $\pm 0.15$ ) nm.<sup>7</sup>

The electron beam gun used in this investigation has been described previously.<sup>8</sup> Foil lifetime has, however, been increased greatly through the installation of a diverter switch in the last section of the 8  $\Omega$  Blumlein.

A cross-section of the heated laser cell is shown in Figure 1. Electrons ( $E \sim 450$  kV), after passing through a 1 x 15 cm slotted, foil support plate entered the cell (excited volume =  $15 \text{ cm}^3$ ) by penetrating a 0.0015" Inconel 718 foil. Vacuum integrity of the system was maintained by double gasketing the foil using 0.025" diameter high purity Aluminum wire. Heating of the cell and foil was accomplished with four heating rods. Placing the rods in front of and behind the foil helped compensate for radiative losses from the cell and electron window into the e-gun diode. Heating tape was wrapped around the Hg reservoir and all stainless steel tubing leading to the cell. For all of the experiments to be described, the cell temperature was maintained 25-50°C higher than the Hg reservoir temperature. Optical quality sapphire flats were aligned normal to the laser cell's axis (sealed to the laser cell with gold gaskets) and also wrapped with heating tape. The features of the cell in Figure 1 are such that:

- 1) little turbulence of the gaseous laser medium, due to temperature inhomogeneities, was observed and
- 2) no window fogging or foil condensation problems were encountered.

The optical cavity consisted of two external dielectric mirrors of 99.5% reflectivity and 0.1% transmission at 557 nm. Fluorescence and

6

laser emission was monitored axially by an ITT F4018 S-5 photodiode and a Corning  $\lambda > 450$  nm colored glass filter. In addition, spectra were obtained using a Jarrell-Ash 0.75 m monochromator in conjunction with Polaroid Type 55 film. The resolution of the recorded spectra was  $\sim 0.4$  nm for fluorescence and 0.15 nm for laser emission.

The laser cell was evacuated to  $\sim 10^{-5}$  Torr and heated to the operating temperature (250-260°C) for several hours before experiments were conducted. Both the Hg and  $\text{CCl}_4$  were degassed by sublimation using dry ice cooled reservoirs.

A typical oscillogram of  $\text{HgCl}$  ( $B \rightarrow X$ ) fluorescence and laser emission waveforms is shown in Figure 2 for:

$$[\text{Ar}] \approx 3.4 \cdot 10^{19} \text{ cm}^{-3},$$

$$[\text{Xe}] \approx 4.2 \cdot 10^{18} \text{ cm}^{-3},$$

$$[\text{Hg}] \approx 1.81 \cdot 10^{18} \text{ cm}^{-3},$$

$$[\text{CCl}_4] \approx 8.4 \cdot 10^{16} \text{ cm}^{-3},$$

$$T_{\text{cell}} = 300^\circ \text{ C}$$

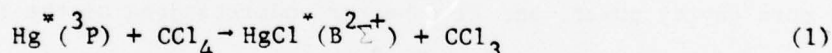
$$\text{and } T_{\text{reservoir}} = 260^\circ \text{ C.}$$

The fluorescence trace has a FWHM of  $\sim 50$  ns and closely follows the e-beam current (not shown). Lasing occurs near the end of the pulse and lasts for  $\sim 20$  ns. For the optical cavity described earlier (0.1% transmitting mirrors), extracted energies of 0.32 mJ/mirror have been observed. Although it is likely that laser output on the order of

of several joules per liter is obtainable for this system, no attempt to optimize the energy output with mirror coupling has been made to date.

Densitometer tracings of the spontaneous emission and laser spectra for the  $\text{HgCl}(B^2\Sigma^+ \rightarrow X^2\Sigma^+)$  system are shown in Figure 3 (gas mixture is the same as before). From the spectra of Wieland<sup>9</sup> and Vikis and LeRoy<sup>10</sup>, the laser lines at 557.62 and 558.35 nm may be tentatively assigned to  $v=0 \rightarrow v'=22$  transitions of the  $B^2\Sigma^+ \rightarrow X^2\Sigma^+$  band of  $\text{HgCl}$ <sup>37</sup> and  $\text{HgCl}$ <sup>35</sup>, respectively. Although  $\text{HgCl}(B^2\Sigma^+)$  transitions are bound-bound, the large Franck-Condon shift of the B and X states<sup>9</sup> suggests that bottlenecking of the lower laser level is minimal and given sufficiently rapid quenching of the  $\text{HgCl}(X^2\Sigma, v'=22)$  state, long pulse operation of this laser may be feasible.

As mentioned previously, formation of  $\text{HgCl}^*(B^2\Sigma^+)$  molecules occurs through the process:<sup>5</sup>

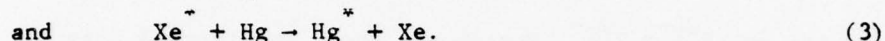
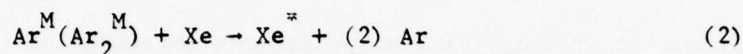


which is exothermic for only the  $\text{Hg}^*(^3P_2)$  state at 5.463 eV. Therefore, collisional quenching of  $\text{Hg}^*(^3P_2)$  to  $\text{Hg}^*(^3P_1)$  or  $^3P_0$  is detrimental to this mercury-halide laser. Fortunately, the cross-section for this process is small for quenching of  $\text{Hg}^*(^3P_2)$  by  $\text{CCl}_4$ .<sup>5</sup> However, the absorption at 546 nm which is shown in Figure 3 is due to  $\text{Hg}^*(6^3P_2 \rightarrow 7^3S_1)$  transitions which reduces the laser's efficiency through  $\text{Hg}^*(6^3P_2)$  population depletion.

For the gas mixtures used in these experiments, the electron beam

energy is primarily absorbed by the argon, creating  $\text{Ar}^M$  and  $\text{Ar}_2^M$ .

Subsequently, ground state Hg atoms are excited through the collisional processes:



Fluorescence spectra of electron beam pumped Ar/Xe/Hg/ $\text{CCl}_4$  mixtures, however, reveal strong  $\text{XeCl}(\text{B}^+ \text{X})$  emission at 308 nm, indicating that quenching of  $\text{Xe}^*$  by  $\text{CCl}_4$  is interfering with (3).<sup>11</sup> It was also observed that for  $\text{CCl}_4$  densities in excess of  $10^{17} \text{ cm}^{-3}$ ,  $\text{HgCl}(\text{B}^2\Sigma)$  fluorescence was severely reduced which suggests increased quenching of  $\text{Xe}^*$  and  $\text{HgCl}^*$  by  $\text{CCl}_4$ .

In summary, laser emission on the  $v=0 \rightarrow v'=22$  line of the  $\text{B}^2\Sigma^+ \rightarrow \text{X}^2\Sigma^+$  band of HgCl has been observed. Although the output energies reported here are small, improved performance of the HgCl laser can be anticipated through: 1) the use of higher transmission mirrors to extract more cavity power, and 2) a better understanding of the formation and quenching kinetics of  $\text{HgCl}^*(\text{B}^2\Sigma^+)$ . If lasing is obtained on other members of the HgX family, line-tunable coverage of a majority of the blue-green portion of the visible spectrum is conceivable. Also, the high efficiencies with which Hg  $6^3\text{P}$  metastables are produced in discharges ( $\eta > 50\%$ ) suggests that direct electron impact pumping of  $\text{Hg}^*(6^3\text{P})$  followed by  $\text{HgX}^*$  formation could be an efficient pumping mechanism for this laser. Finally, the high vapor pressure of mercury at moderate temperatures makes the mercury-halide laser family a promising area for future high power laser development.

### References

1. S. K. Searles and G. A. Hart, Appl. Phys. Lett. 27, 243 (1975).
2. J. G. Eden and S. K. Searles, Appl. Phys. Lett. 29, 350 (1976) and references cited.
3. J. A. Mangano and J. H. Jacobs, Appl. Phys. Lett. 27, 495 (1975).
4. N. Djeu and R. Burnham, Appl. Phys. Lett. 30, 473 (1977).
5. H. F. Krause, S. G. Johnson, S. Datz and F. K. Schmidt-Bleek, Chem. Phys. Lett. 31, 577 (1975).
6. D. R. Herschbach, Advan. Chem. Phys. 10, 319 (1966).
7. J. H. Parks has also recently reported the observation of lasing in HgCl: J. H. Parks, postdeadline paper TAI15, 5th Conference on Chemical and Molecular Lasers, St. Louis, MO (April, 1977).
8. J. G. Eden and S. K. Searles, Appl. Phys. Lett. 30, 287 (1977).
9. K. Wieland, Helv. Phys. Acta 14, 420 (1941).
10. A. C. Vikis and D. J. LeRoy, Chem. Phys. Lett. 21, 103 (1973).
11. Quenching of  $\text{Xe}^*$  by  $\text{Cl}_2$  defines, of course, an upper limit for the efficiency of the HgCl laser. The kinetic sequence (see reference 12):  $\text{Ar}^M \rightarrow \text{N}_2(\text{A}) \rightarrow \text{Hg}^*$  might be considered as an alternative scheme for pumping, for example, the  $\text{HgBr}^*$  laser in  $\text{Ar}/\text{N}_2/\text{Hg}/\text{halogen donor}$  mixtures. It is not an acceptable scheme for  $\text{HgCl}^*$ , however, since quenching of  $\text{Hg}(6^3\text{P}_2)$  to  $\text{Hg}(6^3\text{P}_1)$  by  $\text{N}_2$  is rapid (cf. reference 5).
12. C. J. Duthler and H. P. Broida, J. Chem. Phys. 59, 167 (1973).

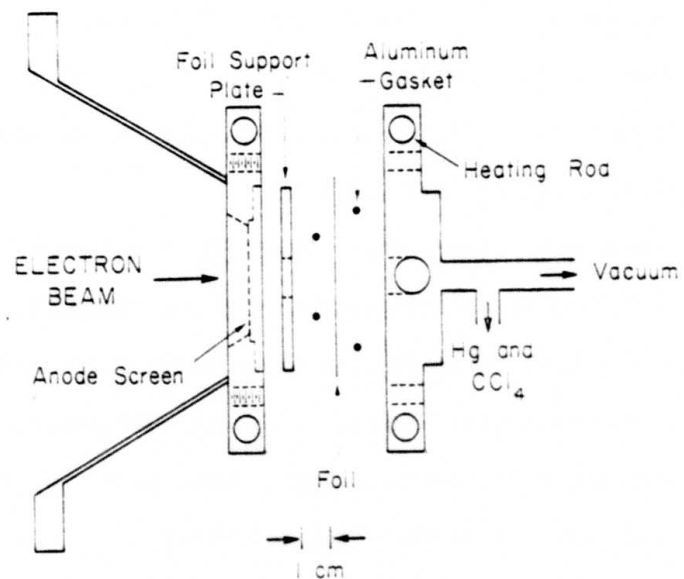


Figure 1. Schematic diagram of a cross-section of the laser cell.

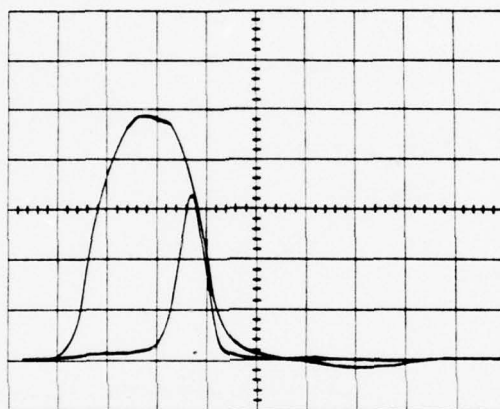


Figure 2. Oscilloscope of typical HgCl(B $\rightarrow$ X) fluorescence and laser emission waveforms. Horizontal scale: 20 ns/div; Vertical units arbitrary.

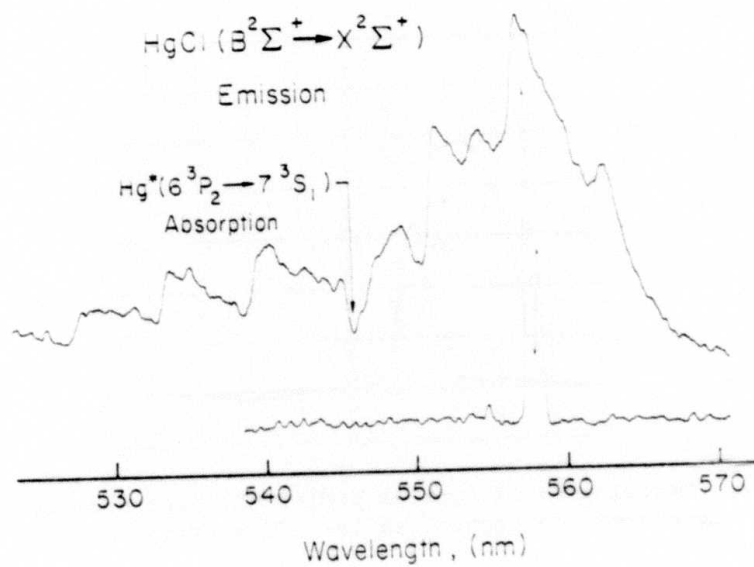


Figure 3. Densitometer tracing of  $\text{HgCl}(B \rightarrow X)$  laser and spontaneous emission spectra (vertical scale linear).